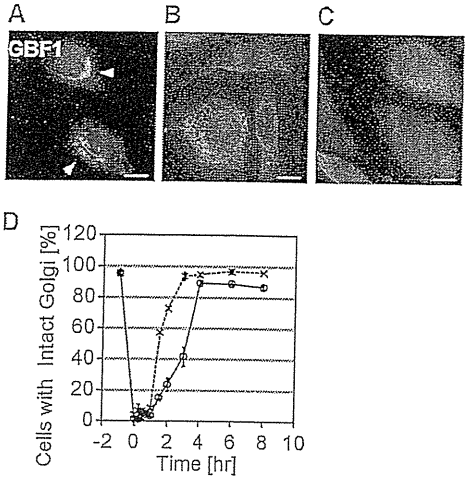

FIGURE 2. **AMF-26 disrupts Golgi apparatus in BSY-1 cells.** *A–C*, dispersion of Golgi in AMF-26-treated cells. BSY-1 cells were either untreated (*A*) or ated with (*B*) BFA (1 μM) or (*C*) AMF-26 (1 μM) for 1 h. Cells were fixed and eled with anti-GBF1 (*green*) and DAPI (*blue*). GBF1 was dispersed from the perinuclear region, which gave a ribbon-like appearance (*white arrowhead*), into the cytoplasm of AMF-26- or BFA-treated cells. *Scale bar*, 20 μm. *D*, BSY-1 cells were treated with AMF-26 (1 μM) or BFA (1 μM) for 1 h, then washed with fresh medium and subsequently cultured without drugs for the indicated time. Thereafter, cells were fixed and stained with an antibody against GBF1. The images were analyzed by MetaMorph software. After the cells were cultured in medium without AMF-26 for 4 h, the normal Golgi structure reappeared in the perinuclear area. Symbols represent the following: *open circle*, AMF-26; *cross*, BFA. *Error bar*, S.D.

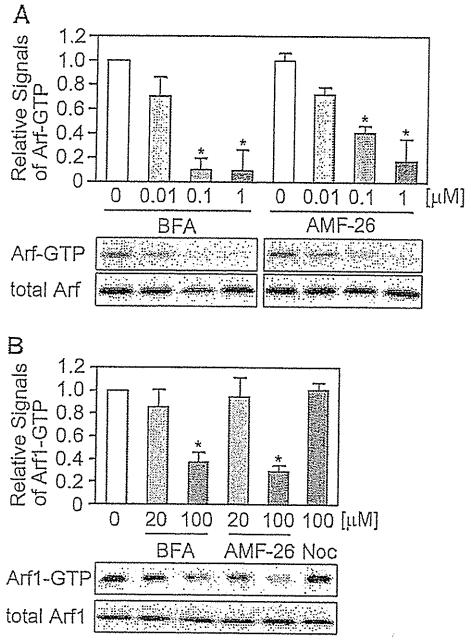

FIGURE 3. **AMF-26 causes the decrease in Arf1 activation.** *A*, BSY-1 cells were treated with DMSO, BFA, or AMF-26 at different concentrations for 1 h after 2 days preincubation. The cells were then lysed, and the extracts were incubated with immobilized GST-GGA3. Bound proteins were released and separated by SDS-PAGE and Western blotted. The signals of endogenous *pan*-Arfs-GTP was determined from the band intensity using ImageJ software. Treatment with AMF-26 or BFA for 1 h dramatically reduced the signals of endogenous *pan*-Arf-GTP in a dose-dependent manner. The relative signals of *pan*-Arf-GTP are represented as the mean of three different experiments. *B*, HEK293T cells transfected transiently with ARF1-HA for 24 h were exposed to DMSO, BFA, AMF-26, or nocodazole at the indicated concentrations for 1 h before lysis. The signals of exogenous Arf1-GTP were determined. Statistical analysis (Student's *t* test) was performed based on experiments done in triplicate. *Asterisks* represent statistically significant differences from untreated samples ($p < 0.05$). Abbreviations represent the following: *BFA*, brefeldin A; *Noc*, nocodazole. *Error bar*, S.D.

AMF-26-induced disruption of Golgi was a reversible process. The normal Golgi structure reappeared in the perinuclear area 4 h after washout of drugs with drug-free medium (Fig. 2*D*), which indicated that the effect of AMF-26 against Golgi was fully reversible like that of BFA (49).

Several tubulin polymerization inhibitors (*e.g.* nocodazole and vincristine) and ionophores (*e.g.* bafilomycin A1 and monensin) are known to disperse the Golgi apparatus (50, 51) as a consequence of disrupting microtubules (supplemental Fig. S1*C*) or intracellular pH (supplemental Fig. S1*F*). However, AMF-26 had no apparent effect on the structure of tubulin pplemental Fig. S1*B*) or localization of lysosomes (supplemental Fig. S1*E*), suggesting that Golgi disruption induced by AMF-26 did not result from the disruption of microtubules or an alteration of intracellular pH.

Inhibition of Arf1 Activation by AMF-26 in Human Cells—By analogy to BFA, we reasoned that the disruption of Golgi via AMF-26 might be mediated through Arf1 inactivation. Then we measured the Arf activity in AMF-26-treated cells by an Arf-GTP pulldown assay that monitored the signals of Arf-GTP using the rGST-GGA3 protein (25, 26). The GAT domain of GGA3, an effector of Arf, preferentially binds the active Arf-GTP over the inactive Arf-GDP (25, 26). Treatment with AMF-26 or BFA for 1 h dramatically reduced the signals of endogenous *pan*-Arf-GTP in a dose-dependent manner within a range of submicromolar concentrations compared with the control state (Fig. 3*A*).

To further confirm that AMF-26 inhibited the activation of Arf1, we evaluated the signals of the exogenous Arf1 in HEK293T cells transiently transfected with human Arf1-HA. The signals of exogenous Arf1-GTP in the AMF-26 or BFA-treated cells for 1 h was significantly reduced in a dose-dependent manner compared with the control cells (Fig. 3*B*). At a concentration of 100 μM, AMF-26 and BFA reduced the signals of exogenous Arf1-GTP to 28.6 and 37.1%, respectively. These data suggested that AMF-26 caused Golgi disassembly by blocking Arf1 activation.

Comparison between the BFA and AMF-26 Complexes—To support this conclusion, we performed computer modeling/MD simulations. The octahydronaphthalene ring of AMF-26 (HP1, HP2, and DA1) was superimposed onto the lactone ring of BFA (HP1, HP2, and HA1) by SUPERPOSE (Fig. 4*C*). During the MD trajectory, the octahydronaphthalene ring of AMF-26 resided in the initial position. The refined model of the Arf1-AMF-26-Sec7 domain complex was compared with the X-ray structure of the Arf1-BFA-Sec7 domain complex (Fig. 4, *D* and *E*, supplemental Table S2). The same hydrophobic residues (Val-53, Thr-64, Trp-66, and Tyr-81 of Arf1 and Met-194, Thr-197, and Val-204 of Sec7 domain) interacted with the octahydronaphthalene ring of AMF-26 and the lactone ring of BFA. The hydrophobic interactions correspond to the matching of hydrophobic property spheres (HP1 and HP2) by SUPERPOSE. The positively charged Arg-19 of Arf1 interacted with the hydroxyl oxygen of AMF-26 and the carbonyl oxygen of BFA. This electrostatic interaction accounted for the match-

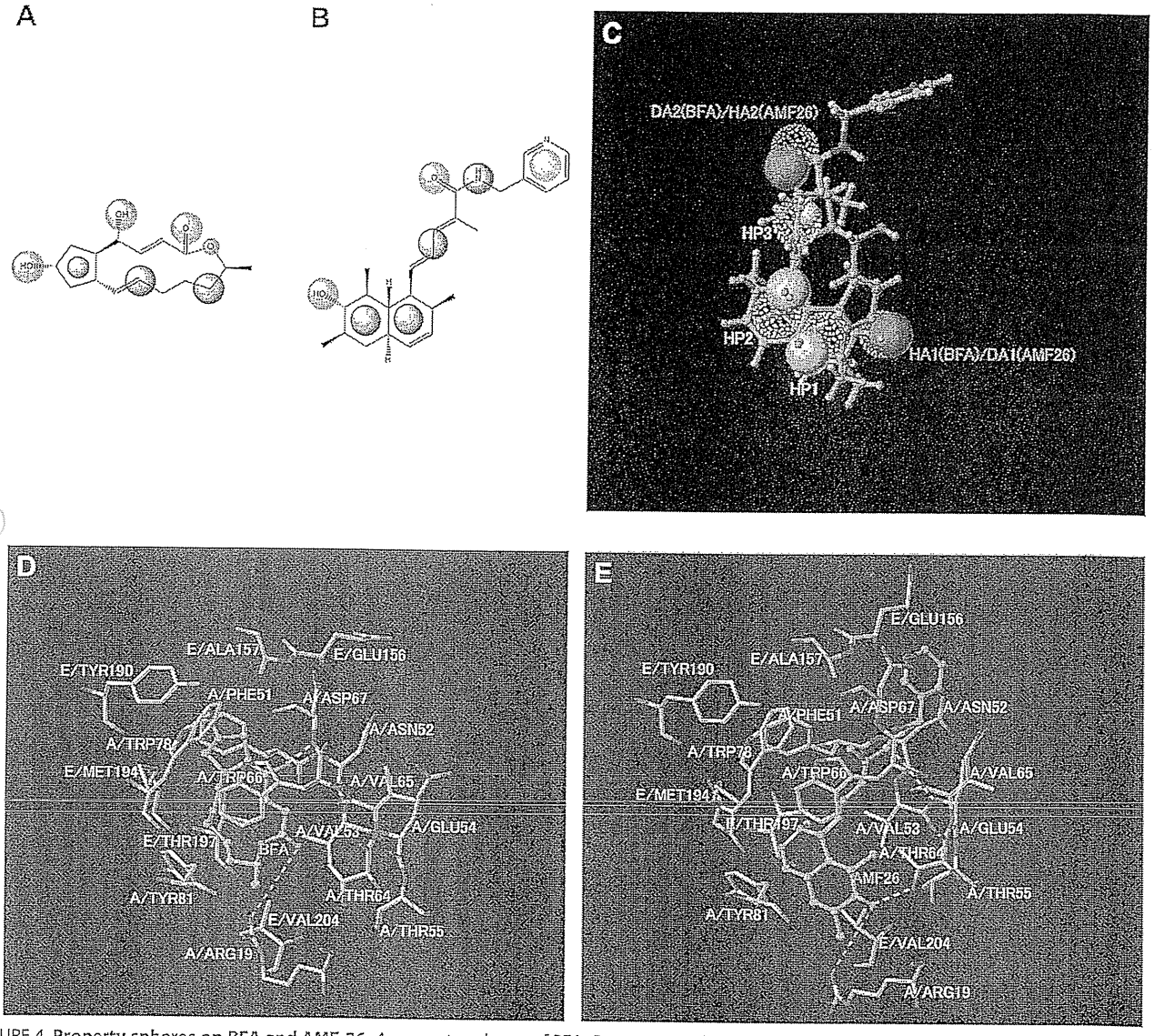

FIGURE 4. **Property spheres on BFA and AMF-26.** *A*, property spheres of BFA. *B*, property spheres of AMF-26. The *spheres* on each molecule are property spheres for molecular superposition. The colors of the spheres indicate the following properties: hydrophobic (HP; *black*), aromatic (AR; *green*), hydrogen-bond donors (HD; *blue*), hydrogen-bond acceptors (HA; *red*), and hydrogen-bond donors/acceptor (DA; *purple*). *Large* and *small spheres* indicate radii of 1 and 0.5 Å, respectively. *C*, superimposition of AMF-26 on BFA by the SUPERPOSE program. AMF-26 is shown in *green*, and BFA is shown in *orange*. Sphere colors indicate the following properties: hydrophobic (*white*), aromatic (*green*), hydrogen-bond donors (*blue*), hydrogen-bond acceptors (*red*), and hydrogen-bond donors/acceptor (*purple*). *Large* and *small spheres* represent radii of 1 and 0.5 Å, respectively. The AMF-26 and BFA spheres are represented by *dotted* and *solid spheres*, respectively. Only matched spheres are indicated. *D* and *E*, comparison between the BFA and AMF-26 complexes. *D*, X-ray structure of the Arf1-BFA-Sec7 domain complex (PDB ID 1r8q). *E*, refined model of the Arf1-AMF-26-Sec7 domain complex. *A* and *E* chains are Arf1 and Sec7 domain, respectively. The hydrogen bonds and the electrostatic interactions are indicated by *yellow* and *pink dashed lines*, respectively.

ing of hydrogen-bond acceptors (DA1 of AMF-26 and HA1 of BFA). In addition, the hydroxyl group of AMF-26 hydrogen-bonded to the side chain of Thr-64 of Arf1. Instead of the hydrogen bond between the hydroxyl oxygen of the lactone ring of BFA and the amide nitrogen of Asp-67 of Arf1, the amide oxygen of AMF-26 hydrogen-bonded with the main chain of Glu-54 of Arf1. This computer modeling/MD simulation suggested that AMF-26 bound to the contact surface of the Arf1-Sec7 domain where BFA is known to bind.

Effects of AMF-26 on the cis-Golgi, TGN, and Recycling Endosomes—To clarify the mechanism of Golgi disruption by AMF-26, we first examined the effect of AMF-26 on localization of *cis*-Golgi-associated proteins, βCOPI, GBF1, and p58/ERGIC53. COPI is the most important coat protein in facilitating retrograde intracellular transport from Golgi to the endoplasmic reticulum (ER) (52). In control cells, most of the βCOPI was localized on the *cis*-Golgi membrane, whereas the addition of AMF-26 caused a rapid release of βCOPI into the cytoplasm (Fig. 5*A*). GBF1, primarily localized in *cis*-Golgi as shown in Fig. 2, was dispersed into the cytoplasm of cells treated with AMF-26. Furthermore, treatment with AMF-26 caused the redistribution of p58/ERGIC53, a marker for the ER-Golgi intermediate compartment (*ERGIC*) (53), from its normal compact localization to a dispersed cytoplasmic

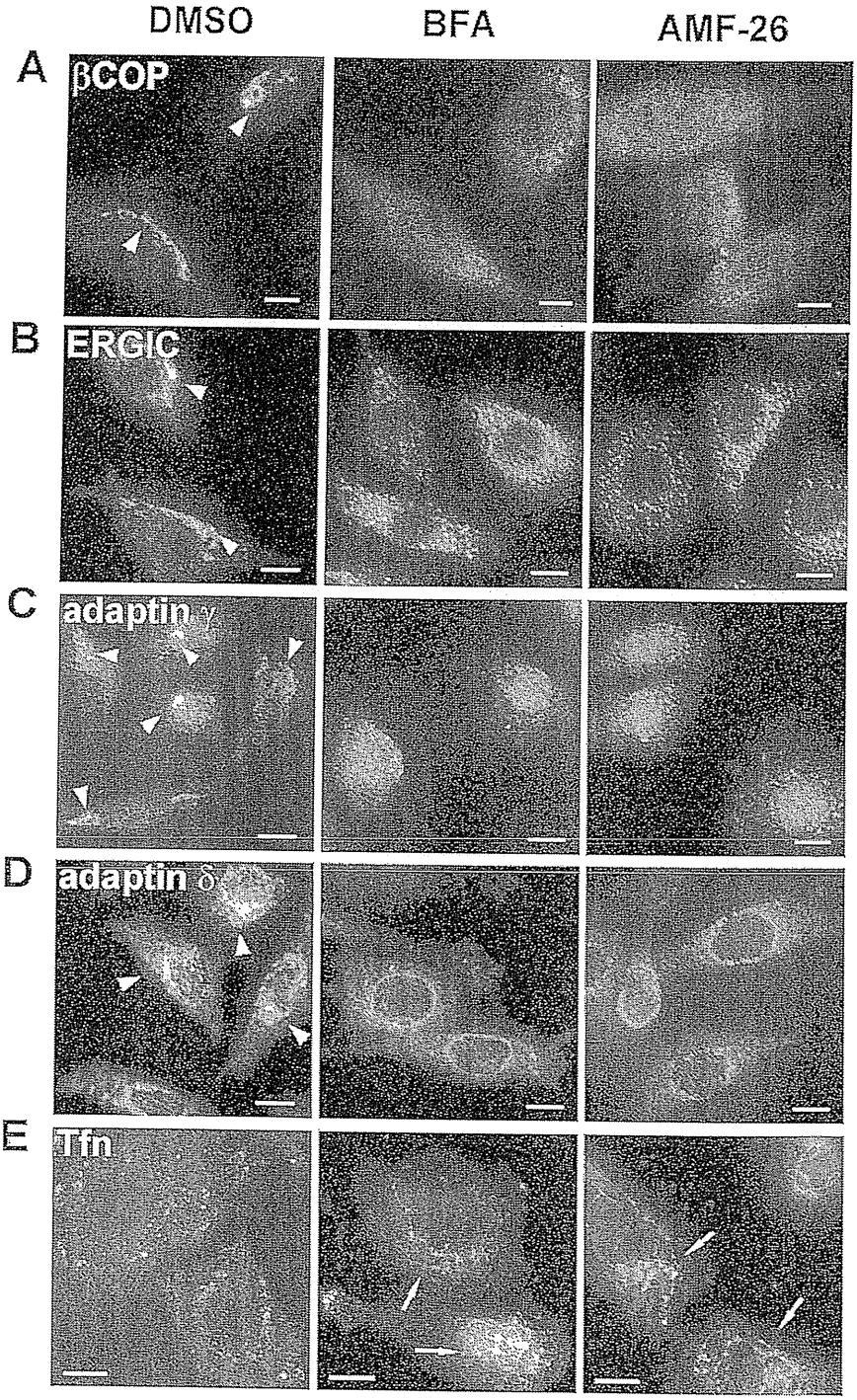

FIGURE 5. **Effects of AMF-26 on *cis*-Golgi, TGN, and recycling endosomes.** BSY-1 cells were incubated with DMSO, BFA (1 μM), or AMF-26 (1 μM) for 1 h. The labeling with each Golgi marker protein (*white*) was as follows: *A*, β-COP (*cis*-Golgi); *B*, ERGIC-53 (*cis*-Golgi and ERGIC); *C*, adaptin γ (TGN); or *D*, adaptin δ (TGN). The localization of *cis*-Golgi and TGN resulted in redistribution from the perinuclear region (*white arrowhead*) into the cytosol. *Scale bar*, 20 μm. *E*, BSY-1 cells were incubated with Alexa 488-labeled transferrin (*white*) for 1 h, and then treated with DMSO, BFA (1 μM), or AMF-26 (1 μM) for 1 h. AMF-26 induced extensive formation of membrane tubules from endosomes (*white arrow*). A similar result was found with BFA. *Scale bar*, 10 μm.

localization (Fig. 5*B*). These effects were similar to those of BFA.

We also examined the effects of AMF-26 on proteins associated with the TGN. AMF-26 affected adaptin γ or adaptin δ, constituents of AP-1 or AP-2, respectively (54), and eventually resulted in redistribution from the perinuclear region into the cytosol (Fig. 5, *C* and *D*).

Concerning recycling endosomes, treatment of BFA is known to induce extensive formation of membrane tubules from endosomes (10, 55). Using Alexa 488-labeled transferrin,

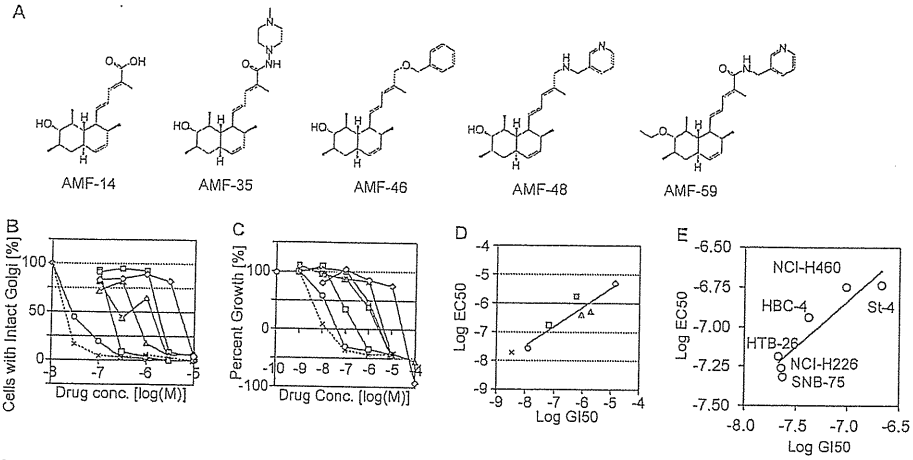

FIGURE 6. **Correlation between cell growth inhibition and Golgi disruption.** *A*, chemical structures of AMF-26 derivatives: AMF-14, AMF-35, AMF-46, AMF-48, and AMF-59. *B*, BSY-1 cells were treated with DMSO, AMF-26, and its derivatives, or BFA at different concentrations for 1 h, and then stained with antibodies against GBF-1. The numbers of cells whose Golgi was dispersed were then counted. Over 100 features were measured under each condition. *C*, the proliferation of BSY-1 cells treated with drugs was monitored as described above. Changes in the amounts of total cellular protein after 48 h of drug treatment were analyzed using the sulforhodamine B assay. *D*, Golgi dispersal activities were correlated with growth inhibitory activities between AMF-26 and its derivatives (Pearson correlation coefficients; $r = 0.92$, $p = 0.009$). Symbols represent the following: *open circle*, AMF-26; *open square*, AMF-48; *closed square*, AMF-59; *open triangle*, AMF-46; *closed triangle*, AMF-14; *open diamond*, AMF-35; cross, BFA-treated cells. *E*, Golgi dispersal activities were correlated with growth inhibitory activities between six cell lines of JFCR39 (Pearson correlation coefficients, $r = 0.93$, $p = 0.02$).

we analyzed the effect of AMF-26 on the formation of tubular endosomes. AMF-26 induced enlargement and tubulation of transferrin-positive endosomes (Fig. 5*E*), suggesting that AMF-26 has a similar effect on early/recycling endosomes as BFA.

Correlation between Cell Growth Inhibition and Golgi Disruption—It is still uncertain whether the growth-inhibitory activity of BFA is related to its effects on Golgi disruption (56, 57). We examined the correlation between cell growth inhibition and Golgi disruption activity to investigate the causal relationship of these two events. Specifically, we examined the activities of AMF-26 and its five derivatives AMF-14, AMF-35, AMF-46, AMF-48, and AMF-59 (structural formula of each compound shown in Fig. 6*A*). In BSY-1 cells, AMF-26 exhibited the strongest activity of cell growth inhibition with a GI_{50} of 12 nM and that of Golgi disruption with an EC_{50} of 27 nM. AMF-35 displayed the weakest activities with a GI_{50} and EC_{50} of 14 and [illegible] μM, respectively, (Fig. 6, *B* and *C*). We next investigated whether the Golgi disruption activities (the logarithm of EC_{50}) of these six compounds were related to their growth inhibitory activities (the logarithm of GI_{50}). Our analysis revealed a statistically significant correlation ($r = 0.92$ and $p = 0.009$) between these two activities (Fig. 6*D*). A statistically significant correlation between the logarithm of EC_{50} and the logarithm of GI_{50} was also observed when six other cell lines were treated with AMF-26 ($r = 0.93$ and $p = 0.02$, Fig. 6*E*). Taken together, our results suggested that there was a causal relationship between the Golgi disruption and cell growth inhibition.

AMF-26 Caused Apoptotic Cell Death—After a 24-h incubation with AMF-26, the sub-G_1 population increased in a dose-dependent manner over that of the DMSO-treated controls, *i.e.* 8.4 (AMF-26, 100 nM) *versus* 1.9% (Fig. 7*A*). These differences in the sub-G_1 population were even greater after 48 h, *i.e.* AMF-26-treated cells 13.1 (AMF-26, 100 nM) *versus* 2.1% (Fig. 7*A*). Furthermore, cleavage products of PARP were assessed by Western blot analysis of cell lysates (Fig. 7*B*). After incubation for 24 h, a band corresponding to cleaved PARP (89-kDa) was significantly stronger in cell extracts of AMF-26-treated cells compared with DMSO-treated cells. After 48 h, the larger accumulation of cleaved PARP in AMF-26-treated cells was obvious, suggesting apoptosis of AMF-26-treated cells.

Analysis of the Antitumor Efficacy of Orally Administrated AMF-26 Using Xenografts of Human Breast Cancer BSY-1—Finally, we evaluated the antitumor activity of AMF-26 against human breast cancer BSY-1 xenografts. After formation of the tumors (100–300 mm^3), mice were orally administered 0 (control vehicle), 83, or 100 mg/kg of AMF-26 for 5 consecutive days. Administration of AMF-26 at 83 or 100 mg/kg induced almost complete tumor regression on day 21 (Fig. 7*C*, *upper panel*). To assess toxicity, we measured the body weight of the tumor-bearing mice. The weight of the tumor-bearing mice was slightly reduced by administration of AMF-26. After termination of the administration, the weight was rapidly regained but was not fully recovered during the observation (Fig. 7*C*, *lower panel*). These data suggested that AMF-26 treatment did not cause serious irreversible side effects.

DISCUSSION

In this study, we identified a novel Golgi disruptor, AMF-26 using COMPARE analysis followed by computer modeling/MD simulation and biological validations. AMF-26 is thought to induce Golgi disruption via the inhibition of Arf1 activation. The Golgi disrupting activity of AMF-26 was significantly correlated with its growth-inhibiting activity. Finally, our results showed that oral administration of AMF-26 induced the regression of human breast cancer BSY-1 xenografts.

The Arf family of small GTPases plays a major role in maintaining Golgi structure and driving Golgi membrane traffic (5, 7). It is known that the BFA-sensitive large ArfGEFs, such as GBF1, BIG1, and BIG2, are predominantly localized to the *cis*-Golgi and TGN. After activation by GBF1, Arf1 mediates COPI

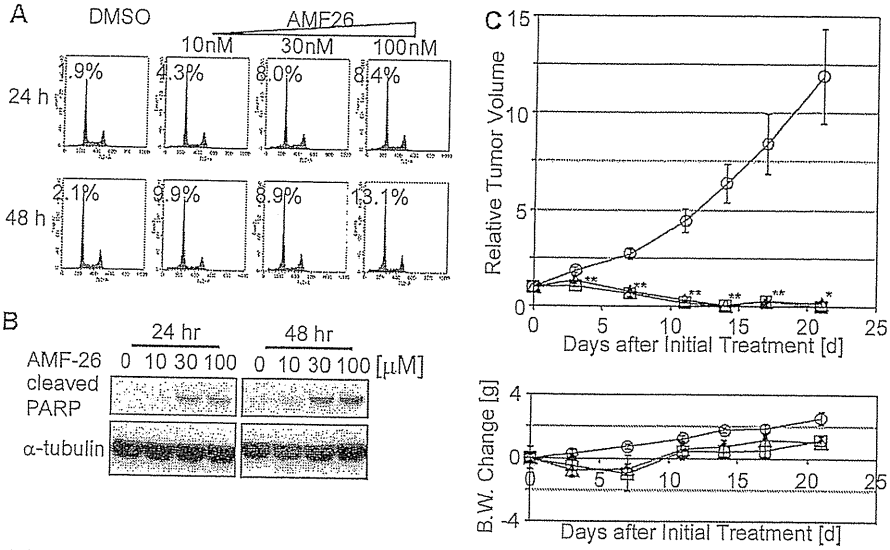

URE 7. **Antitumor activity of AMF-26.** *A* and *B*, AMF-26 caused apoptosis on BSY-1 cell. *A*, cells were incubated with DMSO or with AMF-26 for 24 or 48 h. ...centages of the sub-G_1 population are indicated. AMF-26 influenced the sub-G_1 population in a dose-dependent manner. *B*, effect of AMF-26 on PARP cleavage. BSY-1 cells were incubated with AMF-26 for 24 or 48 h. Cells were lysed and the proteins in the cell extract were separated by SDS-PAGE and electroblotted onto a membrane. The membrane was then probed with antibodies against cleaved PARP and α-tubulin. Cleaved PARP protein was observed in AMF-26-treated cells. *C*, tumor growth and body weight in nude mice bearing human breast cancer BSY-1 xenografts. Fifteen nude mice were subcutaneously inoculated with a tumor fragment of 3 × 3 × 3 mm from the subcutaneous tumor developed in nude mice. When tumors reached a volume of 100–300 mm^3, animals were divided randomly into test groups, each with five mice (day 0). AMF-26 (83 or 100 mg/kg) was orally administered daily from day 0 to 5. AMF-26 data are the means of data from five mice. The *upper panel* shows the relative tumor volume. The *lower panel* shows the body weight change. Administration of AMF-26 induced complete tumor regression on day 21. *Asterisks* represent statistically significant differences from the control group (*, $p < 0.01$; **, $p < 0.005$). Symbols represent the following: *open circle*, control vehicle; *open square*, AMF-26 (83 mg/kg); *open triangle*, AMF-26 (100 mg/kg) was orally administrated group; *error bar*, S.E.

coat recruitment and enables vesicle transport between Golgi and ER (48). On the other hand, when activated by BIG1 or BIG2, Arf1 recruits adapter proteins, AP-1, AP-3, and AP-4(58), and Golgi-associated γ-adaptin ear-containing Arf-binding proteins, GGA1, GGA2, and GGA3 (59). These Arf1-effector molecules mediate transport between TGN and endosomes (58). BFA inactivates Arf1 by inhibiting PPIs between Arf1 and Arf1GEFs, and subsequently induces the disruption of *cis*-Golgi and TGN, or affects the endosomal systems (10, 11). Furthermore, BFA showed tumor growth inhibition *in vitro* (12) and *in vivo* at an early stage (13). From the viewpoint of developing molecular-targeted drugs, BFA is attractive because ...target, Arf1 and ArfGEF interaction, is unique. However, BFA and its derivatives have not progressed beyond the preclinical stage of drug development (13, 14).

Here we used COMPARE analysis to screen for compounds showing a BFA-like fingerprint, and identified AMF-26. BFA has a lactone ring, whereas AMF-26 has an octahydronaphthalene ring with a side chain including a pyridine moiety. Although the chemical structure of AMF-26 is distinct from that of BFA, we verified that the two compounds share a similar molecular mode of action as expected from the COMPARE analysis. Moreover, computer modeling/MD simulation and biological validations suggested that AMF-26 inhibited the interaction between Arf1 and BFA-sensitive large ArfGEFs. AMF-26 induced the disruption of *cis*-Golgi and TGN at almost the same concentrations as BFA, and inhibited recycling of transferrin. These results indicate that AMF-26 is a novel inhibitor of Arf1 activation whose chemical structure is different from BFA.

Several other Golgi disruptors related to Arf activation have been reported (44, 57, 60–62). These compounds showed inhibition of membrane traffic. However, their precise modes of action appear to be different from that of AMF-26 and BFA. Moreover, compared with AMF-26 or BFA, these compounds resulted in much weaker inhibition of cell growth.

It remains uncertain whether cell growth inhibition by BFA arises from Golgi disruption. Citterio *et al.* (56) indicated that decreased expression of GBF1, BIG1, or BIG2 by siRNA caused dispersion of the Golgi-localized protein and the inhibition of cell growth. We observed similar results in BSY-1 cells in our preliminary data.[3] However, Pan *et al.* (57) reported that AG1478 showed a weak loss of cell viability. In the present study, we demonstrated that AMF-26 inhibited both Arf1 activation and tumor cell growth in BSY-1 cells. Moreover, AMF-26 and its derivatives showed a positive correlation between the Golgi-disrupting activity and the cell growth-inhibiting activity. We also found a positive correlation between the two when six other cancer cell lines were treated with AMF-26. In our preliminary experiments, inactivation of the phosphatidylinositol 3-kinase pathway or Ras-MAPK pathway was not observed by exposure of cells to AMF-26 for 10 min (data not shown). Collectively, our results suggested a causal relationship between Golgi disruption and cell growth inhibition by AMF-26. Furthermore, in the present study, we found that AMF-26 induced apoptosis in tumor cells. Our observations agree with the report of Citterio *et al.* (56) indicating that decreased expression of GBF1 causes apoptosis.

A previous study described the antitumor activity of BFA in early stage mouse subcutaneous models (13). In the course of

[3] Y. Ohashi, H. Iijima, N. Yamaotsu, K. Yamazaki, S. Sato, M. Okamura, K. Sugimoto, S. Dan, and T. Yamori, unpublished data.

these studies, BFA was injected intraperitoneally twice a day. Frequent administration was necessary because the clearance of BFA is rapid (less than 20 min) (13), consistent with the observation that this compound is a substrate of glutathione *S*-transferase (63). Here, we demonstrated that oral administration of AMF-26 once a day induced almost complete regression of human breast cancer BSY-1 xenografts in nude mice. To the best of our knowledge, this is the first report describing the oral administration of an inhibitor targeting Arf1 activation that elicits strong antitumor activity without severe body weight loss. Further study on the pharmacokinetic profile of AMF-26 remains to be performed.

Very recently, AMF-26 was identified as an angiogenesis inhibitor by Watari *et al.* (64), who revealed that inhibition of VEGF receptor phosphorylation and NF-κB signaling was involved in antiangiogenic activity in human umbilical vein endothelial cells. Therefore, the *in vivo* antitumor activity of AMF-26 shown in the present study may have partly resulted from its antiangiogenic activity in addition to its direct tumor growth inhibition.

The COMPARE analysis is a powerful tool that can be used to identify small-molecule enzyme inhibitors, for example, telomerase inhibitor (FJ-5002) (45), a topoisomerase I and II inhibitor (MS-247) (19), and PI3K inhibitor (ZSTK474) (22, 46, 47). In this study, we exploited the COMPARE analysis to screen BFA-like small molecule inhibitors. Using this approach, we identified AMF-26 as a novel inhibitor of Arf1 activation, despite the fact that its chemical structure does not resemble that of BFA. From these results, the screening of chemicals guided by COMPARE analysis appears to be useful for the discovery of novel drug candidates targeting various biological functions including the Golgi system.

In conclusion, we identified a novel Golgi disruptor targeting Arf1 activation, AMF-26, and showed that it induced complete regression of human breast cancer BSY-1 xenografts. These data suggest that AMF-26 is a novel drug candidate for cancer treatment targeting Arf1 activation.

Acknowledgments—We thank Dr. R. H. Shoemaker and Dr. K. D. Paull for discussion on the establishment of JFCR39 and COMPARE analysis; Y. Nishimura, M. Seki, Y. Mukai, and Y. Yamazaki for technical assistance; NIPPON SHINYAKU CO., Ltd. for provision of AMF-26 and its derivatives and for discussion concerning the nature of the compounds; and Dr. S Sakaushi (Osaka Prefecture University, Osaka, Japan) for advice on time lapse analysis.

REFERENCES

1. Berg, T. (2008) Small-molecule inhibitors of protein-protein interactions. *Curr. Opin. Drug Discov. Devel.* 11, 666–674
2. Wells, J. A., and McClendon, C. L. (2007) Reaching for high-hanging fruit in drug discovery at protein-protein interfaces. *Nature* 450, 1001–1009
3. Lauria, A., Tutone, M., Ippolito, M., Pantano, L., and Almerico, A. M. (2010) Molecular modeling approaches in the discovery of new drugs for anti-cancer therapy. The investigation of p53-MDM2 interaction and its inhibition by small molecules. *Curr. Med. Chem.* 17, 3142–3154
4. Azmi, A. S., and Mohammad, R. M. (2009) Non-peptidic small molecule inhibitors against Bcl-2 for cancer therapy. *J. Cell Physiol.* 218, 13–21
5. D'Souza-Schorey, C., and Chavrier, P. (2006) ARF proteins. Roles in membrane traffic and beyond. *Nat. Rev. Mol. Cell Biol.* 7, 347–358
6. Mossessova, E., Gulbis, J. M., and Goldberg, J. (1998) Structure of the guanine nucleotide exchange factor Sec7 domain of human arno and analysis of the interaction with ARF GTPase. *Cell* 92, 415–423
7. Casanova, J. E. (2007) Regulation of Arf activation. The Sec7 family of guanine nucleotide exchange factors. *Traffic* 8, 1476–1485
8. Renault, L., Guibert, B., and Cherfils, J. (2003) Structural snapshots of the mechanism and inhibition of a guanine nucleotide exchange factor. *Nature* 426, 525–530
9. Zeeh, J. C., Zeghouf, M., Grauffel, C., Guibert, B., Martin, E., Dejaegere, A., and Cherfils, J. (2006) Dual specificity of the interfacial inhibitor brefeldin A for ARF proteins and Sec7 domains. *J. Biol. Chem.* 281, 11805–11814
10. Lippincott-Schwartz, J., Yuan, L., Tipper, C., Amherdt, M., Orci, L., and Klausner, R. D. (1991) Brefeldin A effects on endosomes, lysosomes, and the TGN suggest a general mechanism for regulating organelle structure and membrane traffic. *Cell* 67, 601–616
11. Lippincott-Schwartz, J., Yuan, L. C., Bonifacino, J. S., and Klausner, R. D. (1989) Rapid redistribution of Golgi proteins into the ER in cells treated with brefeldin A. Evidence for membrane cycling from Golgi to ER. *Cell* 56, 801–813
12. Häcki, J., Egger, L., Monney, L., Conus, S., Rossé, T., Fellay, I., and Borner, C. (2000) Apoptotic cross-talk between the endoplasmic reticulum and mitochondria controlled by Bcl-2. *Oncogene* 19, 2286–2295
13. Sausville, E. A., Duncan, K. L., Senderowicz, A., Plowman, J., Randazzo, P. A., Kahn, R., Malspeis, L., and Grever, M. R. (1996) Antiproliferative effect *in vitro* and antitumor activity *in vivo* of brefeldin A. *Cancer J. Sci. Am.* 2, 52–58
14. Anadu, N. O., Davisson, V. J., and Cushman, M. (2006) Synthesis and anticancer activity of brefeldin A ester derivatives. *J. Med. Chem.* 49, 3897–3905
15. Monks, A., Scudiero, D., Skehan, P., Shoemaker, R., Paull, K., Vistica, D., Hose, C., Langley, J., Cronise, P., and Vaigro-Wolff, A. (1991) Feasibility of a high-flux anticancer drug screen using a diverse panel of cultured human tumor cell lines. *J. Natl. Cancer Inst.* 83, 757–766
16. Paull, K. D., Shoemaker, R. H., Hodes, L., Monks, A., Scudiero, D. A., Rubinstein, L., Plowman, J., and Boyd, M. R. (1989) Display and analysis of patterns of differential activity of drugs against human tumor cell lines. Development of mean graph and COMPARE algorithm. *J. Natl. Cancer Inst.* 81, 1088–1092
17. Shoemaker, R. H. (2006) The NCI60 human tumor cell line anticancer drug screen. *Nat. Rev. Cancer* 6, 813–823
18. Yamori, T. (2003) Panel of human cancer cell lines provides valuable database for drug discovery and bioinformatics. *Cancer Chemother. Pharmacol.* 52, Suppl. 1, S74–79
19. Yamori, T., Matsunaga, A., Sato, S., Yamazaki, K., Komi, A., Ishizu, K., Mita, I., Edatsugi, H., Matsuba, Y., Takezawa, K., Nakanishi, O., Kohno, H., Nakajima, Y., Komatsu, H., Andoh, T., and Tsuruo, T. (1999) Potent antitumor activity of MS-247, a novel DNA minor groove binder, evaluated by an *in vitro* and *in vivo* human cancer cell line panel. *Cancer Res.* 59, 4042–4049
20. Dan, S., Tsunoda, T., Kitahara, O., Yanagawa, R., Zembutsu, H., Katagiri, T., Yamazaki, K., Nakamura, Y., and Yamori, T. (2002) An integrated database of chemosensitivity to 55 anticancer drugs and gene expression profiles of 39 human cancer cell lines. *Cancer Res.* 62, 1139–1147
21. Sharma, S. V., Haber, D. A., and Settleman, J. (2010) Cell line-based platforms to evaluate the therapeutic efficacy of candidate anticancer agents. *Nat. Rev. Cancer* 10, 241–253
22. Yaguchi, S., Fukui, Y., Koshimizu, I., Yoshimi, H., Matsuno, T., Gouda, H., Hirono, S., Yamazaki, K., and Yamori, T. (2006) Antitumor activity of ZSTK474, a new phosphatidylinositol 3-kinase inhibitor. *J. Natl. Cancer Inst.* 98, 545–556
23. Sakaushi, S., Senda-Murata, K., Fukada, T., Oka, S., and Sugimoto, K. (2007) Rhythmic cycle of clathrin-coated pit formation at the *trans*-Golgi network in human MDA-MB-435 cells. *Biosci. Biotechnol. Biochem.* 71, 571–574
24. Skehan, P., Storeng, R., Scudiero, D., Monks, A., McMahon, J., Vistica, D., Warren, J. T., Bokesch, H., Kenney, S., and Boyd, M. R. (1990) New colorimetric cytotoxicity assay for anticancer drug screening. *J. Natl. Cancer Inst.* 82, 1107–1112

25. Takatsu, H., Yoshino, K., Toda, K., and Nakayama, K. (2002) GGA proteins associate with Golgi membranes through interaction between their GGAH domains and ADP-ribosylation factors. *Biochem. J.* 365, 369–378
26. Puertollano, R., Randazzo, P. A., Presley, J. F., Hartnell, L. M., and Bonifacino, J. S. (2001) The GGAs promote ARF-dependent recruitment of clathrin to the TGN. *Cell* 105, 93–102
27. Tsujishita, H., and Hirono, S. (1997) CAMDAS, an automated conformational analysis system using molecular dynamics. Conformational analyzer with molecular dynamics and sampling. *J. Comput. Aided Mol. Des.* 11, 305–315
28. Halgren, T. A. (1999) MMFF VI. MMFF94s option for energy minimization studies. *J. Comput. Chem.* 20, 720–729
29. Halgren, T. A. (1999) MMFF VII. Characterization of MMFF94, MMFF94s, and other widely available force fields for conformational energies and for intermolecular-interaction energies and geometries. *J. Comput. Chem.* 20, 730–748
30. Iwase, K., and Hirono, S. (1999) Estimation of active conformations of drugs by a new molecular superposing procedure. *J. Comput. Aided Mol. Des.* 13, 499–512
31. Cornell, W. D., Cieplak, P., Bayly, C. I., Gould, I. R., Merz, K. M., Jr., Ferguson, D. M., Spellmeyer, D. C., Fox, T., Caldwell, J. W., and Kollman, P. A. (1995) A second generation force field for the simulation of proteins, nucleic acids, and organic molecules. *J. Am. Chem. Soc.* 117, 5179–5197
32. Gasteiger, J., and Marsili, M. (1980) Iterative partial equalization of orbital electronegativity—a rapid access to atomic charges. *Tetrahedron* 36, 3219–3228
33. Gasteiger, J., and Marsili, M. (1981) Prediction of proton magnetic resonance shifts: the dependence on hydrogen charges obtained by iterative partial equalization of orbital electronegativity. *Organ. Magn. Reson.* 15, 353–360
34. Marsili, M., and Gasteiger, J. (1980) Pi-charge distributions from molecular topology and pi-orbital electronegativity. *Croat. Chem. Acta* 53, 601–614
35. Purcel, W. P., and Singer, J. A. (1967) A brief review and table of semiempirical parameters used in the Hueckel molecular orbital method. *J. Chem. Eng. Data* 12, 235–246
36. Case, D. A., Darden, T. A., Cheatham, T. E., III, Simmerling, C. L., Wang, J., Duke, R. E., Luo, R., Merz, K. M., Pearlman, D. A., Crowley, M., Walker, R. C., Zhang, W., Wang, B., Hayik, S., Roitberg, A., Seabra, G., Wong, K. F., Paesani, F., Wu, X., Brozell, S., Tsui, V., Gohlke, H., Yang, L., Tan, C., Mongan, J., Hornak, V., Cui, G., Beroza, P., Mathews, D. H., Schafmeister, C., Ross, W. S., and Kollman, P. A. (2006) *AMBER* 9, University of California, San Francisco, CA
37. Wang, J., Cieplak, P., and Kollman, P. A. (2000) How well does a restrained electrostatic potential (RESP) model perform in calculating conformational energies of organic and biological molecules? *J. Comput. Chem.* 21, 1049–1074
38. Wang, J., Wolf, R. M., Caldwell, J. W., Kollman, P. A., and Case, D. A. (2004) Development and testing of a general Amber force field. *J. Comput. Chem.* 25, 1157–1174
39. Cieplak, P., Cornel, W. D., Bayly, C., and Kollman, P. A. (1995) Application of the multimolecule and multiconformational RESP methodology to biopolymers: Charge derivation for DNA, RNA, and proteins. *J. Comput. Chem.* 16, 1357–1377
40. Frisch, M. J., Trucks, G. W., Schlegel, H. B., Scuseria, G. E., Robb, M. A., Cheeseman, J. R., Montgomery, Jr., J. A., Vreven, T., Kudin, K. N., Burant, J. C., Millam, J. M., Iyengar, S. S. T. J., Barone, V., Mennucci, B., Cossi, M., Scalmani, G., Rega, N., Petersson, G. A., Nakatsuji, H., Hada, M., Ehara, M., Toyota, K., Fukuda, R., Hasegawa, J., Ishida, M., Nakajima, T., Honda, Y., Kitao, O., Nakai, H., Klene, M., Li, X., Knox, J. E., Hratchian, H. P., Cross, J. B., Bakken, V., Adamo, C., Jaramillo, J., Gomperts, R., Stratmann, R. E., Yazyev, O., Austin, A. J., Cammi, R., Pomelli, C., Ochterski, J. W., Ayala, P. Y., Morokuma, K., Voth, G. A., Salvador, P., Dannenberg, J. J., Zakrzewski, V. G., Dapprich, S., Daniels, A. D., Strain, M. C., Farkas, O., Malick, D. K., Rabuck, A. D., Raghavachari, K., Foresman, J. B., Ortiz, J. V., Cui, Q., Baboul, A. G., Clifford, S., Cioslowski, J., Stefanov, B. B., Liu, G., Liashenko, A., Piskorz, P., Komaromi, I., Martin, R. L., Fox, D. J., Keith, T., Al-Laham, M. A., Peng, C. Y., Nanayakkara, A., Challacombe, M., Gill, P. M., Johnson, B., Chen, W., Wong, M. W., Gonzalez, C., and Pople, J. A. (2004) *Gaussian 03, Revision C.02*, Gaussian, Inc., Wallingford, CT
41. Jorgensen, W. L., Chandrasekhar, J., Madura, J., and Klein, M. L. (1983) Comparison of simple potential functions for simulating liquid water. *J. Chem. Phys.* 79, 926–935
42. Darden, T., York, D., and Pedersen, L. (1993) Particle mesh Ewald: An N·log(N) method for Ewald sums in large systems. *J. Chem. Phys.* 98, 10089–10092
43. Ryckaert, J. P., Ciccotti, G., and Berendsen, H. J. (1977) Numerical integration of the cartesian equations of motion of a system with constraints: molecular dynamics of n-alkanes. *J. Comput. Phys.* 23, 327–341
44. Sáenz, J. B., Sun, W. J., Chang, J. W., Li, J., Bursulaya, B., Gray, N. S., and Haslam, D. B. (2009) Golgicide A reveals essential roles for GBF1 in Golgi assembly and function. *Nat. Chem. Biol.* 5, 157–165
45. Naasani, I., Seimiya, H., Yamori, T., and Tsuruo, T. (1999) FJ5002, a potent telomerase inhibitor identified by exploiting the disease-oriented screening program with COMPARE analysis. *Cancer Res.* 59, 4004–4011
46. Dan, S., Okamura, M., Seki, M., Yamazaki, K., Sugita, H., Okui, M., Mukai, Y., Nishimura, H., Asaka, R., Nomura, K., Ishikawa, Y., and Yamori, T. (2010) Correlating phosphatidylinositol 3-kinase inhibitor efficacy with signaling pathway status. *In silico* and biological evaluations. *Cancer Res.* 70, 4982–4994
47. Kong, D., Dan, S., Yamazaki, K., and Yamori, T. (2010) Inhibition profiles of phosphatidylinositol 3-kinase inhibitors against PI3K superfamily and human cancer cell line panel JFCR39. *Eur. J. Cancer* 46, 1111–1121
48. Niu, T. K., Pfeifer, A. C., Lippincott-Schwartz, J., and Jackson, C. L. (2005) Dynamics of GBF1. A brefeldin A-sensitive Arf1 exchange factor at the Golgi. *Mol. Biol. Cell* 16, 1213–1222
49. Thyberg, J., and Moskalewski, S. (1999) Role of microtubules in the organization of the Golgi complex. *Exp. Cell Res.* 246, 263–279
50. Morré, D. J., Minnifield, N., and Mollenhauer, H. H. (1985) Kinetics of monensin-induced swelling of Golgi apparatus cisternae of H-2 hepatoma cells. *Eur. J. Cell Biol.* 37, 107–110
51. Thyberg, J., and Moskalewski, S. (1989) Subpopulations of microtubules with differential sensitivity to nocodazole. Role in the structural organization of the Golgi complex and the lysosomal system. *J. Submicrosc. Cytol. Pathol.* 21, 259–274
52. Presley, J. F., Ward, T. H., Pfeifer, A. C., Siggia, E. D., Phair, R. D., and Lippincott-Schwartz, J. (2002) Dissection of COPI and Arf1 dynamics *in vivo* and role in Golgi membrane transport. *Nature* 417, 187–193
53. Appenzeller-Herzog, C., and Hauri, H. P. (2006) The ER-Golgi intermediate compartment (ERGIC). In search of its identity and function. *J. Cell Sci.* 119, 2173–2183
54. Nakayama, K., and Wakatsuki, S. (2003) The structure and function of GGAs, the traffic controllers at the TGN sorting cross-roads. *Cell Struct. Funct.* 28, 431–442
55. Wood, S. A., Park, J. E., and Brown, W. J. (1991) Brefeldin A causes a microtubule-mediated fusion of the *trans*-Golgi network and early endosomes. *Cell* 67, 591–600
56. Citterio, C., Vichi, A., Pacheco-Rodriguez, G., Aponte, A. M., Moss, J., and Vaughan, M. (2008) Unfolded protein response and cell death after depletion of brefeldin A-inhibited guanine nucleotide-exchange protein GBF1. *Proc. Natl. Acad. Sci. U.S.A.* 105, 2877–2882
57. Pan, H., Yu, J., Zhang, L., Carpenter, A., Zhu, H., Li, L., Ma, D., and Yuan, J. (2008) A novel small molecule regulator of guanine nucleotide exchange activity of the ADP-ribosylation factor and Golgi membrane trafficking. *J. Biol. Chem.* 283, 31087–31096
58. Ishizaki, R., Shin, H. W., Mitsuhashi, H., and Nakayama, K. (2008) Redundant roles of BIG2 and BIG1, guanine-nucleotide exchange factors for ADP-ribosylation factors in membrane traffic between the *trans*-Golgi network and endosomes. *Mol. Biol. Cell* 19, 2650–2660
59. Doray, B., Ghosh, P., Griffith, J., Geuze, H. J., and Kornfeld, S. (2002) Cooperation of GGAs and AP-1 in packaging MPRs at the *trans*-Golgi network. *Science* 297, 1700–1703
60. Viaud, J., Zeghouf, M., Barelli, H., Zeeh, J. C., Padilla, A., Guibert, B., Chardin, P., Royer, C. A., Cherfils, J., and Chavanieu, A. (2007) Structure-based discovery of an inhibitor of Arf activation by Sec7 domains through targeting of protein-protein complexes. *Proc. Natl. Acad. Sci. U.S.A.* 104,

10370–10375
61. Feng, Y., Yu, S., Lasell, T. K., Jadhav, A. P., Macia, E., Chardin, P., Melancon, P., Roth, M., Mitchison, T., and Kirchhausen, T. (2003) Exo1, a new chemical inhibitor of the exocytic pathway. *Proc. Natl. Acad. Sci. U.S.A.* 100, 6469–6474
62. Feng, Y., Jadhav, A. P., Rodighiero, C., Fujinaga, Y., Kirchhausen, T., and Lencer, W. I. (2004) Retrograde transport of cholera toxin from the plasma membrane to the endoplasmic reticulum requires the *trans*-Golgi network but not the Golgi apparatus in Exo2-treated cells. *EMBO Rep.* 5, 596–601
63. Brüning, A., Ishikawa, T., Kneusel, R. E., Matern, U., Lottspeich, F., and Wieland, F. T. (1992) Brefeldin A binds to glutathione *S*-transferase and is secreted as glutathione and cysteine conjugates by Chinese hamster ovary cells. *J. Biol. Chem.* 267, 7726–7732
64. Watari, K., Nakamura, M., Fukunaga, Y., Furuno, A., Shibata, T., Kawahara, A., Hosoi, F., Kuwano, T., Kuwano, M., and Ono, M. (2011) The antitumor effect of a novel angiogenesis inhibitor (an octahydronaphthalene derivative) targeting both VEGF receptor and NF-κB pathway. *Int. J. Cancer* doi: 10.1002/ijc.26356

EUROPEAN JOURNAL OF CANCER 48 (2012) 936–943

Available at www.sciencedirect.com

SciVerse ScienceDirect

journal homepage: www.ejconline.com

ZSTK474, a specific phosphatidylinositol 3-kinase inhibitor, induces G1 arrest of the cell cycle *in vivo*

Shingo Dan [a], *Mutsumi Okamura* [a], *Yumiko Mukai* [a], *Hisashi Yoshimi* [a,c], *Yasumichi Inoue* [b], *Aki Hanyu* [b], *Asako Sakaue-Sawano* [d,e], *Takeshi Imamura* [b,f], *Atsushi Miyawaki* [d,e], *Takao Yamori* [a,*]

[a] *Division of Molecular Pharmacology, Cancer Chemotherapy Center, Japanese Foundation for Cancer Research, 3-8-31 Ariake, Koto-ku, Tokyo 135-8550, Japan*

[b] *Division of Biochemistry, Cancer Institute, Japanese Foundation for Cancer Research, 3-8-31 Ariake, Koto-ku, Tokyo 135-8550, Japan*

[c] *Research Laboratory, Zenyaku Kogyo, Co. Ltd., Ohizumi-machi, Nerima-ku, Tokyo, Japan*

[d] *Laboratory for Cell Function and Dynamics, Advanced Technology Development Group, Brain Science Institute, RIKEN, 2-1 Hirosawa, Wako-city, Saitama 351-0198, Japan*

[e] *Life Function and Dynamics, ERATO, JST, 2-1 Hirosawa, Wakò-city, Saitama 351-0198, Japan*

[f] *Department of Molecular Medicine for Pathogenesis, Ehime University Graduate School of Medicine and CREST, JST, Shitsukawa, Toon, Ehime 791-0295, Japan*

ARTICLE INFO

Article history:
Available online 14 November 2011

Keywords:
Phosphatidylinositol 3-kinase (PI3K) inhibitor
ZSTK474
G1 arrest of the cell cycle
Antitumour agents
in vivo imaging

ABSTRACT

Phosphatidylinositol 3-kinase (PI3K) is regarded as a promising therapeutic target because it is often activated in cancer. We previously reported that ZSTK474, a specific PI3K inhibitor, inhibits tumour cell proliferation *via* G1 arrest of the cell cycle without inducing apoptosis *in vitro*. However, it remained unclear whether ZSTK474 induces G1 arrest to exert antitumour efficacy *in vivo*. We recently developed a live imaging system, named Fluorescent Ubiquitination-based Cell Cycle Indicator (Fucci), to visualise cell cycle distribution. Here, by using this system, we tested whether ZSTK474 induces G1 arrest in tumour cells *in vivo*, as well as *in vitro*. Fucci-introduced human breast cancer MCF-7 cells and cervical cancer HeLa cells were subcutaneously xenografted in nude mice. ZSTK474 was administered to the tumour-bearing mice for 5 days, and the cell cycle distribution in the xenografted tumours were analysed by monitoring fluorescence in live mice. We demonstrate that ZSTK474 induces G1arrest along with tumour suppression *in vivo*. Moreover, we show that ZSTK474 suppresses the tumour growth without inducing apoptosis. Interestingly, such increase in G1 cells and tumour suppression was maintained during long-term (3-month) administration of ZSTK474. These results suggest that ZSTK474 exerts its *in vivo* antitumour efficacy *via* G1 arrest but not *via* apoptosis as long as it is administered, and could be used for months as maintenance therapy for patients with advanced cancers.

1. Introduction

The PI3K pathway is frequently activated in cancer by a gain-of-function hotspot mutation of the *PIK3CA* gene[1,2] and loss of Phosphatase and Tensin homolog deleted on chromosome 10 (PTEN) expression,[3,4] thereby activating tumourigenesis and tumour growth. Thus, PI3K is thought to be a promising target for cancer therapy. We previously reported a selective PI3K

* *Corresponding author:* Tel.: +81 3 3520 0111; fax: +81 3 3570 0484.
E-mail address: yamori@jfcr.or.jp (T. Yamori).

0959-8049/$ - see front matter © 2011 Elsevier Ltd. All rights reserved.
doi:10.1016/j.ejca.2011.10.006

inhibitor ZSTK474 with potent antitumour activity and low toxicity *in vivo*.[5–7] Subsequently, a number of PI3K inhibitors have been developed, and some, including ZSTK474 and NVP-BEZ235, have already entered clinical trials.[8–12]

Inhibition of the PI3K pathway was expected to induce apoptosis, cell cycle arrest and cell growth inhibition. However, in our previous study, we demonstrate that inhibition of PI3K by ZSTK474 induces strong G1 arrest of the cell cycle but scarcely any apoptosis *in vitro*.[6] Consistent with these findings, NVP-BEZ235, a dual PI3K/mammalian Target Of Rapamycin (mTOR) inhibitor, induced G1 arrest but not apoptosis *in vitro*.[13,14] Moreover, we demonstrated that tumour cells did not undergo apoptosis upon administration of ZSTK474 in tumour xenografts derived from various types of human cancers implanted in nude mice.[6] Therefore, the antitumour efficacy of PI3K inhibitors appears to be exerted by a cytostatic mechanism *via* G1 arrest. However, the studies with regard to G1 arrest by PI3K inhibitors were performed *in vitro*. Thus, it remains unclear whether PI3K inhibitors also induce G1 arrest *in vivo*.

We previously developed an imaging system, named Fluorescent Ubiquitination-based Cell Cycle Indicator (Fucci), to visualise cell cycle distribution in living cells by introducing fluorescent cell cycle-specific marker proteins using a lentiviral expression vector.[15] Here, we used the Fucci system to investigate cell cycle distribution after administration of ZSTK474 both *in vivo* and *in vitro*.

2. Materials and methods

2.1. *Cell lines and cell culture*

Human breast cancer MCF-7 cells expressing mCherry-hCdt1 (30/120) and mAG-hGeminin (1/110) and cervical cancer HeLa cells expressing mKO-hCdt1 and mAG-hGeminin were described previously.[15] These cells were grown in Dulbecco's Modified Eagle Medium (DMEM) medium (Wako Pure Chemical Industries Ltd., Osaka, Japan) supplemented with 5% v/v heat-inactivated foetal bovine serum (FBS) (Moregate Exports, Bulimba, Queensland, Australia) and 1 μg/mL kanamycin. Cells were incubated at 37 °C in a humidified atmosphere supplemented with 5% CO_2. Authentication of cell lines was performed by short tandem repeat analysis using PowerPlex16 Systems (Promega, Madison, WI) (data not shown).

2.2. *Drugs*

ZSTK474 was kindly provided by Zenyaku Kogyo Co., Ltd. (Tokyo, Japan). NVP-BEZ235 and GDC-0941 were purchased from Selleck (Houston, TX) and Symansis (Timaru, New Zealand), respectively. Paclitaxel and cisplatin were purchased from Sigma–Aldrich (St. Louis, MO) and Nippon Kayaku (Tokyo, Japan), respectively.

2.3. *Real-time visualisation of cell cycle progression using a fluorescence microscope*

Fucci-introduced cells were seeded at 3.5×10^4 cells/well in a 12-well glass-bottomed plate, and incubated overnight in a CO_2 incubator. Cells were administered with the indicated drugs and cell cycle progression was successively monitored (every 15 min) using a IX81 fluorescence microscope (Olympus, Tokyo, Japan).

2.4. *Animal experiments and in vivo visualisation of the cell cycle*

Animal care and treatment was performed in accordance with the guidelines of the animal use and care committee of the Japanese Foundation for Cancer Research, and conformed to the National Institutes of Health (NIH) Guide for the Care and Use of Laboratory Animals. Female nude mice with BALB/c genetic backgrounds were purchased from Charles River Japan (Yokohama, Japan). Mice were maintained under specific pathogen-free conditions and provided with sterile food and water *ad libitum*. Tumour xenografts were generated by subcutaneously inoculating 1.5×10^7 cells suspended in 100 μL of Hanks' Balanced Salt Solution (Gibco BRL) at each of two sites per mouse. Daily oral administration of ZSTK474 (400 mg/kg) was started when tumour size reached 100–300 mm^3. Length (L) and width (W) of the subcutaneous tumour mass were measured every other day using a pair of calipers. The tumour volume (TV) was calculated as: $TV = (L \times W^2)/2$. Cell cycle distribution in tumours implanted in nude mice was monitored each day 4 h after drug administration by using an OV100 *in vivo* fluorescent imaging system (Olympus). Fluorescence intensity was quantified by using Image J software (National Institute of Health, MD). For microscopic analysis of cell cycle distribution, frozen tumours were fixed in 4% v/v paraformaldehyde and washed with H_2O. Tissue sections (14-μm) were examined using a IX81 fluorescence microscope (Olympus).

2.5. *Immunohistochemistry*

Tumour tissues fixed in 10% neutral formalin were embedded in paraffin. Tissue sections (4-μm) were deparaffinised in xylene and then in a series of (100–50%) ethanol solutions. Specific antibodies against phospho-Akt (Ser-473), phospho-S6, phospho-4E-BP1, phospho-RB (S807/S811) and cleaved PARP (Cell Signalling Technologies, Danvers, MA) were used for hybridization and the bound antibodies were visualised by using DAKO EnVision kit containing a secondary horseradish peroxidase (HRP) conjugated anti mouse polymer antibody complex. Sections were counterstained with Mayer's haematoxylin.

3. Results

3.1. *Real-time visualisation of the induction of G1 arrest in cancer cells after treatment with ZSTK474*

First we examined cell cycle progression *in vitro* after exposure to PI3K inhibitors in human breast cancer MCF-7 cells using the Fucci system (Fig. 1, Supplementary Movies 1 and 2). Control cells exhibited a combination of red and green nuclei and proliferated in parallel to cell cycle progression over a 48 h observation period. Upon exposure to a specific PI3K inhibitor ZSTK474, the number of cells with red nuclei gradually increased and those with green nuclei disappeared within

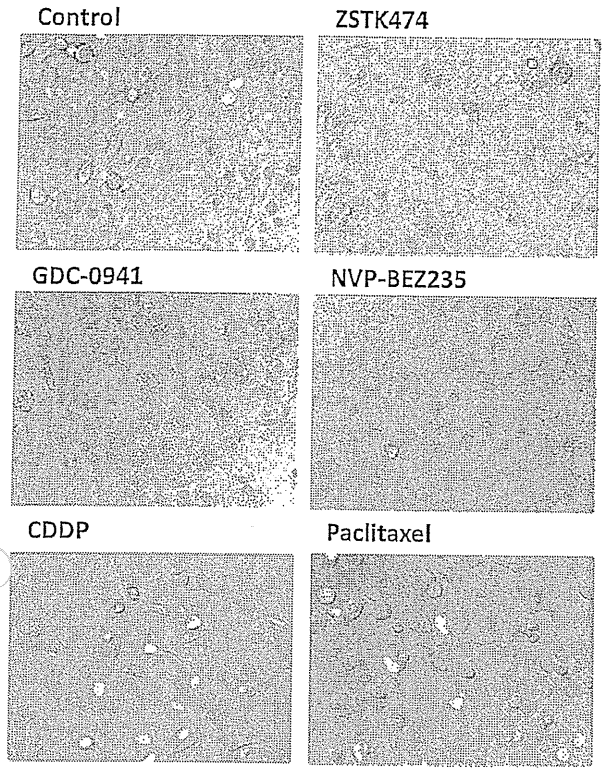

Fig. 1 – *In vitro* visualisation of cell cycle distribution in Fluorescent Ubiquitination-based Cell Cycle Indicator (Fucci)-introduced human breast cancer MCF-7 cells. Fucci-MCF-7 cells were treated with ZSTK474 (5 μM), GDC-0941 (5 μM), NVP-BEZ235 (150 nM), cisplatin (30 μM) or paclitaxel (10 nM) for 24 h. Cell cycle distribution was monitored by using a fluorescence microscope at 24 h after exposure. Red cells in G1 phase increased and green cells in S/G2/M phase decreased upon treatment with phosphatidylinositol 3-kinase (PI3K) inhibitors, but not with cisplatin and paclitaxel.

24 h of exposure to ZSTK474, along with inhibition of cell proliferation. Similar results were obtained when cells were exposed to other PI3K inhibitors GDC-0941 and NVP-BEZ235. Induction of G1 arrest was confirmed by conventional flow cytometric analysis (Fig. S1). However, when cells were treated with cisplatin and paclitaxel, growth inhibition did not coincide with an increase of red nuclei. We next examined the phosphorylation status of PI3K-downstream pathway members including Akt, ribosomal S6 protein (S6) and eukaryotic initiation factor 4E binding protein (4E-BP1). As shown in Fig. S2, these proteins were dephosphorylated after treatment with PI3K inhibitors. Similarly, retinoblastoma protein (Rb) was also dephosphorylated. Interestingly, cleaved poly (ADP ribose) polymerase (PARP) was not detected after treatment with these PI3K inhibitors. Our results show that these PI3K inhibitors inhibit the PI3K pathway, and that hyperphosphorylated Rb protein is reduced in parallel to the induction of G1 arrest of the cell cycle.

3.2. *In vivo imaging of G1 arrest after administration of ZSTK474 in human tumours xenografted in nude mice*

We next carried out *in vivo* analysis of cell cycle after administration of ZSTK474 in xenografted tumours derived from Fucci-MCF7 cells subcutaneously implanted in nude mice. As shown in Fig. 2A, tumour growth was effectively suppressed upon daily administration of ZSTK474 for five days. Macroscopic analyses using the OV100 fluorescence intravital imaging system revealed that the tumours turned from yellow to red as a result of induction of red fluorescence (G1 cells) and the reduction of green fluorescence ($S/G_2/M$ cells) after the second administration of ZSTK474 (Day 2, Fig. 2C). In agreement with this observation, R/G ratio (relative red/green fluorescence intensity ratio) was significantly elevated (Fig. 2B). Microscopic analysis confirmed that the number of green cells dramatically reduced and almost all cells became red in the tumour section resected on Day 5 (Fig. 2D), but no such increase in G1 cells was observed after administration of paclitaxel and cisplatin (data not shown). Similar results were obtained by using xenografted tumours derived from human cervical cancer HeLa cells. These results indicate that the PI3K inhibitor ZSTK474 induces simultaneous G1 cell cycle arrest and suppression of tumour growth *in vivo*.

3.3. *Effect of ZSTK474 on phosphorylation status of PI3K pathway proteins and pRB*

We next examined whether ZSTK474 inhibits the PI3K pathway *in vivo*. As shown in Fig. 3, ZSTK474 reduced the expression levels of phosphorylated Akt, ribosomal S6 protein and 4E-BP1, indicating that the PI3K-Akt-mTOR signalling pathway was indeed inhibited. As expected, ZSTK474 reduced the level of phosphorylated Rb protein in parallel to induction of G1 arrest. Similar results were obtained in xenografted tumours derived from human ovarian cancer SK-OV3 and prostate cancer PC-3 cells after daily administration of ZSTK474 over a two week period (Fig. S3). From these results, we conclude that ZSTK474 inhibits the PI3K pathway during G1 arrest *in vivo*.

3.4. *Antitumour effect of ZSKT474 was not accompanied by apoptosis*

A previous study reported that NVP-BEZ235 selectively induced apoptosis in breast cancer cells carrying a hotspot mutation in the *PIK3CA* gene.[16] Therefore, we attempted to examine the involvement of apoptosis during the tumour regression process induced by ZSTK474 in MCF-7-derived tumours carrying a *PIK3CA* hotspot mutation (E545K). No significant enhancement of apoptotic cells was observed after administration of ZSTK474 as determined by emergence of cleaved PARP (Fig. 3). Similar results were obtained in tumours derived from *PIK3CA*-mutated SK-OV3 cells (H1047R) and those from PTEN-null PC-3 cells (Fig. S3). In agreement with these observations, no enhancement in cleaved PARP was observed when Fucci-MCF7 cells were treated with ZSTK474 *in vitro* (Fig. S2). These results clearly indicate that ZSTK474 exerts a strong *in vivo* antitumour activity against

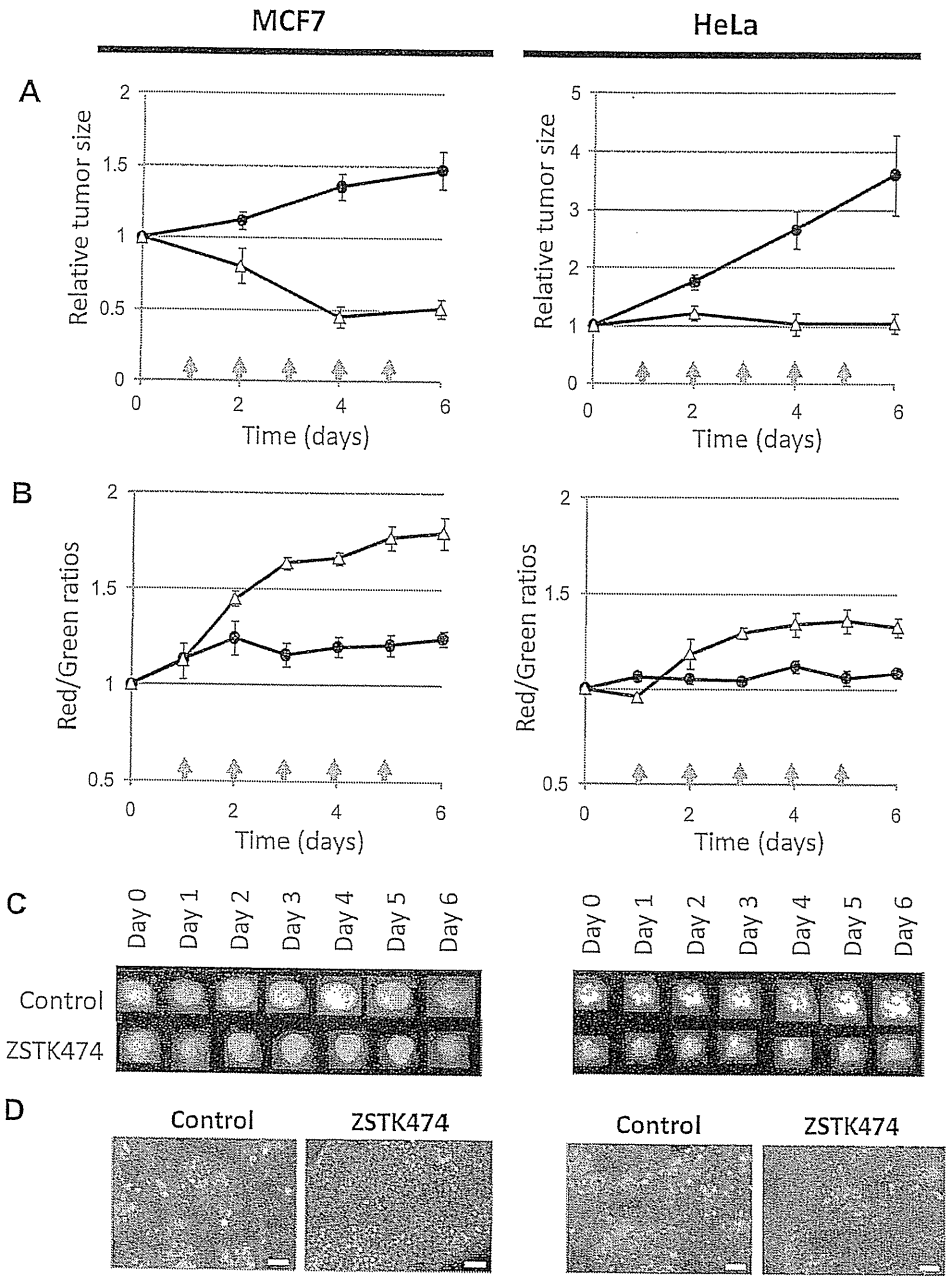

Fig. 2 – *In vivo* visualisation of cell cycle distribution in Fluorescent Ubiquitination-based Cell Cycle Indicator (Fucci)-introduced cancer cells. Fucci-MCF-7 cells and Fucci-HeLa cells were subcutaneously injected in nude mice to generate tumour xenografts. Then, ZSTK474 (400 mg/kg) was orally administered to the tumour-bearing mice ($n = 6$) from Day 1 to Day 5 (as indicated by the red arrows). (A) Tumour sizes in ZSTK474-administered mice ($n = 6$) and control mice ($n = 6$) were measured every other day (4 h after drug administration). Tumour sizes were then normalised to the respective size at day 0. ZSTK474 significantly suppressed tumour growth. (B) Macroscopic analyses using the OV100 fluorescence intravital imaging system were performed to investigate cell cycle distribution in live mice. Red and green fluorescent intensities were measured from each image. Relative fluorescence intensities (R/G ratio) were then calculated. The R/G ratios in each group ($n = 12$) were averaged and the averaged ratio at Day 0 was normalised to 1. (C) Typical images overlaying red and green fluorescence on each day are shown. (D) Microscopic images of frozen tumour sections resected on Day 5 from mice administered with ZSTK474. ZSTK474 drastically reduced the number of green cells with almost all cells turning red. This observation indicates G1 arrest of the cell cycle. Scale bars = 100 μm.

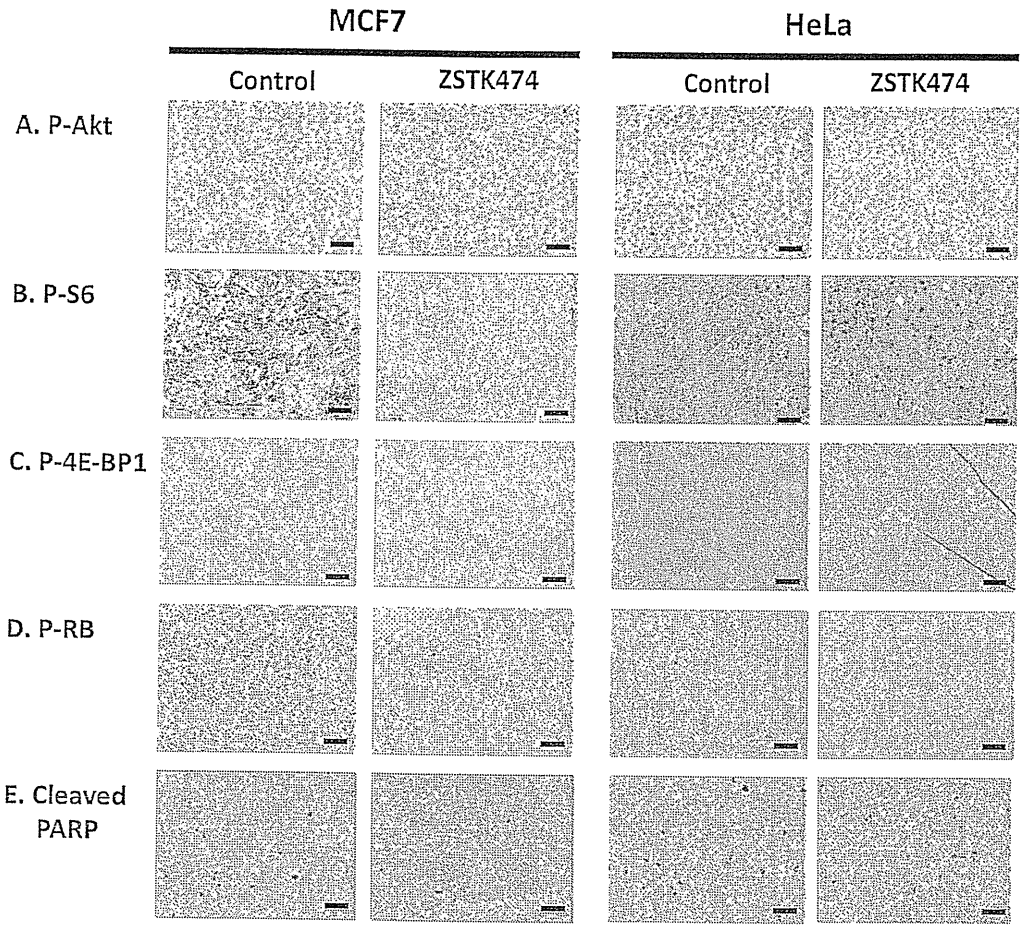

Fig. 3 – *In vivo* effects of ZSTK474 on the phosphorylation levels of phosphatidylinositol 3-kinase (PI3K) pathway members and Rb protein. Tumours derived from Fluorescent Ubiquitination-based Cell Cycle Indicator (Fucci)-MCF-7 cells and Fucci-HeLa cells were resected on Day 5. The sections were then subjected to immunohistochemistry to examine expression levels of phospho-Akt (A), phospho-S6 (B), phospho-4E-BP1 (C) phospho-Rb (D) and cleaved PARP (E) by using specific antibodies for respective proteins. Scale bars = 100 μm.

these *PIK3CA*-mutated and PTEN-deficient tumours without inducing apoptosis.

3.5. *Reduction of cell size after administration of ZSTK474*

Thus far, we have demonstrated that ZSTK474 exerts a strong antitumour activity, and this antitumour effect is accompanied by G1 arrest, but not by apoptosis, despite the observed tumour regression of MCF-7-derived tumours after administration of ZSTK474. A careful investigation of MCF-7-derived tumour sections revealed that tumour cells appeared to shrink after administration of ZSTK474 for five days (Fig. 2D). Therefore, we tested whether ZSTK474 reduced tumour cell size (Fig. 4A and B). Our results clearly show that ZSTK474 significantly increases the tumour cell density. Previous studies have reported that the PI3K pathway regulates cell size *via* mTOR and its downstream targets S6K1 and 4E-BP1.[17] In fact, ZSTK474 reduces cell size in the G1 phase of the cell cycle *in vitro* (Fig. S4) as well as lowering the degree of phosphorylation of S6 and 4E-BP1 both *in vivo* (Fig. 3B and C) and *in vitro* (Fig. S2). Similar results were obtained for SK-OV3- and PC-3-derived tumours (tumour cell density increased by 90% and 32%, respectively. Fig. S3). From these results we concluded that ZSTK474 reduces cell size *in vivo* and *in vitro via* inhibition of S6K1 and 4E-BP1.

3.6. *Accumulation of G1 cells and inhibition of tumour growth during long-term administration of ZSTK474*

In Figs. 2 and S3, we demonstrated that ZSTK474 strongly suppressed tumour growth in parallel to accumulation of G1 cells and/or hypophosphorylation of pRB after daily administration for five days or two weeks. We next attempted to investigate the effect of long-term administration of ZSTK474 on tumour growth and cell cycle distribution. As shown in Fig. 5B, ZSTK474 increased G1 cell population in Fucci-HeLa-derived tumour xenografts within a week, and such increase was maintained during long-term daily administration for up to 100 days. In agreement with this observation, ZSTK474 efficiently blocked tumour growth (Fig. 5A). The result suggested

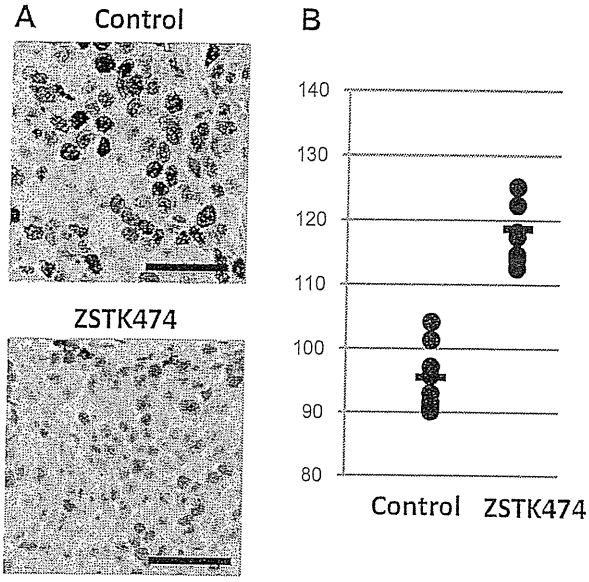

Fig. 4 – Morphological changes of tumour cells derived from Fluorescent Ubiquitination-based Cell Cycle Indicator (Fucci)-MCF7 cells after administration of ZSTK474. (A) Tumours resected on Day 5 were subjected to immunohistochemistry to detect Ki-67. Tumour cells appeared to shrink. Scale bars = 50 μm. (B) Difference in tumour cell densities (i.e. number of tumour cells per unit area) in tumours resected from control mice and those from ZSTK474-administered mice. Data are the averages of eight different fields (2.0×10^4 μm^3) from each sample.

that ZSTK474 exerts its antitumour effect by inducing G1 arrest and this effect lasts at least three months.

4. Discussion

In the current study, we have used the Fucci system to investigate cell cycle distribution in tumours derived from MCF-7 cells and HeLa cells subcutaneously implanted in nude mice after administration of ZSTK474. We have demonstrated for the first time that a PI3K inhibitor ZSTK474 induces G1 arrest in tumour cells *in vivo* in parallel to suppression of tumour growth. We also confirmed that ZSTK474 did not induce apoptosis to exert its *in vivo* antitumour effect, even in *PIK3CA*-mutated tumours. These results suggest that ZSTK474 exerts its antitumour efficacy mainly *via* G1 arrest, but not apoptosis. Moreover, we demonstrated that simultaneous G1 arrest and suppression of tumour growth lasted at least three months as long as daily administration of ZSTK474 continued. These observations indicate that ZSTK474 could be used clinically for controlling tumours in advanced stages. In fact, we previously demonstrated that ZSTK474 strongly inhibited growth of tumours derived from human prostate cancer PC-3 cells xenografted in nude mice, even when the tumour volumes were ~1700 mm^3 in size.[6]

Inhibition of PI3K is believed to induce apoptosis in cancer cells. Indeed, the PI3K inhibitor LY294002 triggered apoptosis in colorectal and pancreatic cancer cells.[18,19] However, previous reports, including our own, have demonstrated that some

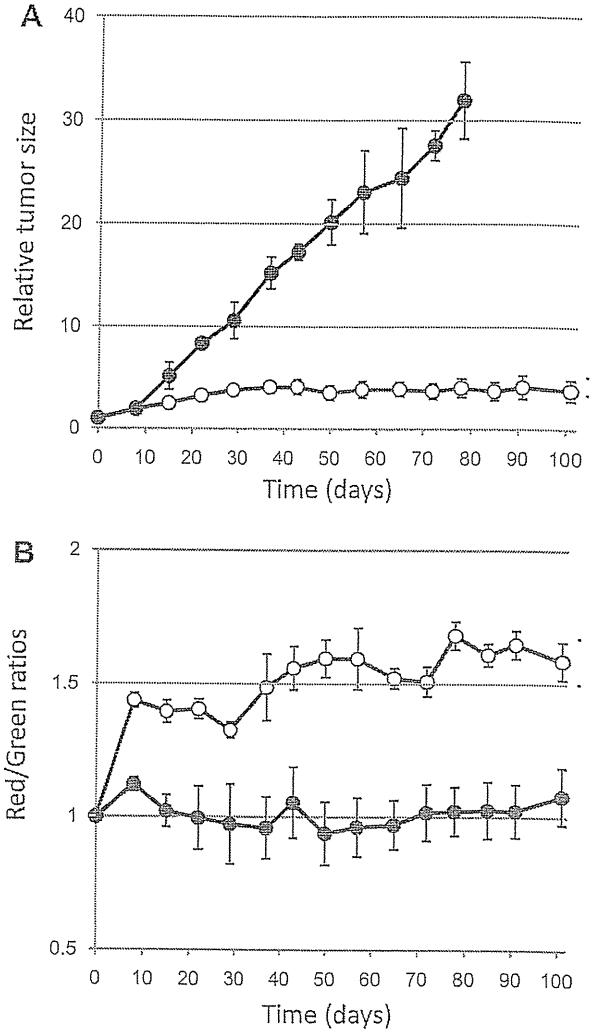

Fig. 5 – Accumulation of G1 cells and inhibition of tumour growth during long-term administration of ZSTK474. Fluorescent Ubiquitination-based Cell Cycle Indicator (Fucci)-HeLa cells were subcutaneously inoculated at each of two sites per mouse ($n = 3$) to generate tumour xenografts. Then, ZSTK474 was orally administered to the tumour-bearing mice from Monday to Friday at a dose of 400 mg/kg (800 mg/kg on Friday). (A) Tumour sizes in ZSTK474-administered mice ($n = 6$) and control mice ($n = 6$) were measured once a week. Measurement of tumour size in control mice was discontinued on day 77 because of the tumour rupture. Tumour sizes were then normalised to the respective size at day 0. (B) Macroscopic analyses using the OV100 fluorescence intravital imaging system were performed to investigate cell cycle distribution in live mice. Red and green fluorescent intensities were measured from each image, and relative fluorescence intensities (R/G ratio) were then calculated. The R/G ratios in each group ($n = 6$) were averaged and the averaged ratio at Day 0 was normalised to 1.

PI3K inhibitors under active development, such as ZSTK474 and NVP-BEZ235, exert their antitumour efficacy *in vitro* by

G1 arrest rather than inducing apoptosis.[5,6,13,14] Recently, NVP-BEZ235 and GDC-0941 were shown to selectively induce apoptosis in breast cancer cells with PI3K mutation and/or Human Epidermal growth factor Receptor 2 (HER2) amplification.[16,20] However, we previously demonstrated that the mutation status of *PIK3CA* did not correlate with the *in vitro* efficacy of ZSTK474 across a panel of 39 human cancer cell lines (JFCR39), nor with the *in vivo* drug efficacies of ZSTK474 across 24 human cancer cell lines implanted in nude mice.[21] In this study, we clearly demonstrate that ZSTK474 induces G1 arrest along with tumour suppression *in vivo* by using Fucci-introduced cancer cells. Moreover, ZSTK474 did not induce apoptosis along with tumour suppression in MCF-7- and SK-OV3-derived tumours despite the fact that these cell lines carry an activating mutation on the *PIK3CA* gene. Of note, SK-OV3 cells overexpress the HER2 protein.[21]

We observed that ZSTK474 reduced tumour cell size during tumour suppression. Previous studies have reported that mTOR regulates cell growth, i.e. cell size in tumour as well as normal cells *via* 4E-BP-1 and S6K1/S6.[17] Indeed, mTOR inhibitors, including CCI-779 and WYE-125132, have been shown to reduce tumour cell size *in vitro* and *in vivo*.[22,23] NVP-BEZ235, a dual inhibitor of PI3 K and mTOR, was also reported to reduce tumour cell size in a mouse model of tuberous sclerosis.[24] In regard to PI3K inhibitors, LY294002 reduced cell size *in vitro*,[17] but LY294002 is not a specific inhibitor of class I PI3Ks, but inhibits a number of protein kinase such as casein kinase 2 and DNA-PK.[10,25] In this study, we clearly demonstrate that a specific PI3K inhibitor ZSTK474 reduces tumour cell size *in vivo* along with a decrease in the level of phosphorylated 4E-BP1 and S6. Our findings suggest that ZSTK474-induced tumour regression is caused in part by tumour cell size reduction. However, further studies are needed to establish the functional involvement of cell size reduction in the efficacy of the antitumour activity of PI3K inhibitors.

In summary, using the Fucci system we have demonstrated that a PI3K inhibitor ZSTK474 induces G1 arrest, but not apoptosis, *in vivo* along with tumour suppression even in tumours carrying a gain-of-function mutation in the *PIK3CA* gene. Moreover, we show that G1 arrest and inhibition of tumour growth induced by ZSTK474 last at least three months as long as ZSTK474 is daily administered to the recipient mice. In addition, we found that ZSTK474 reduces cell size both *in vivo* and *in vitro*. ZSTK474 has entered Phase I clinical trials in U.S. in January 2011, and we expect that ZSTK474 could be used as a maintenance therapy for patients with advanced cancers in future clinical trials.

Conflict of interest statement

Takao Yamori has a research fund from Zenyaku Kogyo Co., Ltd., which is the proprietary company of ZSTK474; H. Yoshimi is an employee of Zenyaku Kogyo Co., Ltd.

Acknowledgements

We thank Zenyaku-Kogyo Co., Ltd. and Dr. Roger Y. Tsien for providing us ZSTK474 and mCherry plasmid, respectively.

This work was supported in part by Grants-in-Aid for Scientific Research (A) from Japan Society for the Promotion of Science to T. Yamori (22240092); Grants-in-Aid for Young Scientists (B) from Japan Society for the Promotion of Science to S. Dan (22700929); Grant-in-Aid for Scientific Research on Innovative Areas, Scientific Support Programs for Cancer Research, from The Ministry of Education, Culture, Sports, Science and Technology of Japan to T. Yamori (221S0001).

Appendix A. Supplementary data

Supplementary data associated with this article can be found, in the online version, at doi:10.1016/j.ejca.2011.10.006.

REFERENCES

1. Samuels Y, Velculescu VE. Oncogenic mutations of *PIK3CA* in human cancers. *Cell Cycle* 2004;3(10):1221–4.
2. Samuels Y, Wang Z, Bardelli A, et al. High frequency of mutations of the *PIK3CA* gene in human cancers. *Science* 2004;304(5670):554.
3. Li J, Yen C, Liaw D, et al. PTEN, a putative protein tyrosine phosphatase gene mutated in human brain, breast, and prostate cancer. *Science* 1997;275(5308):1943–7.
4. Steck PA, Pershouse MA, Jasser SA, et al. Identification of a candidate tumour suppressor gene, MMAC1, at chromosome 10q23.3 that is mutated in multiple advanced cancers. *Nat Genet* 1997;15(4):356–62.
5. Yaguchi S, Fukui Y, Koshimizu I, et al. Antitumor activity of ZSTK474, a new phosphatidylinositol 3-kinase inhibitor. *J Natl Cancer Inst* 2006;98(8):545–56.
6. Dan S, Yoshimi H, Okamura M, Mukai Y, Yamori T. Inhibition of PI3K by ZSTK474 suppressed tumor growth not via apoptosis but G0/G1 arrest. *Biochem Biophys Res Commun* 2009;379(1):104–9.
7. Kong D, Okamura M, Yoshimi H, Yamori T. Antiangiogenic effect of ZSTK474, a novel phosphatidylinositol 3-kinase inhibitor. *Eur J Cancer* 2009;45(5):857–65.
8. Engelman JA. Targeting PI3K signalling in cancer: opportunities, challenges and limitations. *Nat Rev Cancer* 2009;9(8):550–62.
9. Hoeflich KP, O'Brien C, Boyd Z, et al. In vivo antitumor activity of MEK and phosphatidylinositol 3-kinase inhibitors in basal-like breast cancer models. *Clin Cancer Res* 2009;15(14):4649–64.
10. Kong D, Yamori T. Advances in development of phosphatidylinositol 3-kinase inhibitors. *Curr Med Chem* 2009;16(22):2839–54.
11. Kong D, Yamori T. Phosphatidylinositol 3-kinase inhibitors: promising drug candidates for cancer therapy. *Cancer Sci* 2008;99(9):1734–40.
12. Workman P, Clarke PA, Raynaud FI, van Montfort RL. Drugging the PI3 kinome: from chemical tools to drugs in the clinic. *Cancer Res* 2010;70(6):2146–57.
13. Maira SM, Stauffer F, Brueggen J, et al. Identification and characterization of NVP-BEZ235, a new orally available dual phosphatidylinositol 3-kinase/mammalian target of rapamycin inhibitor with potent in vivo antitumor activity. *Mol Cancer Ther* 2008;7(7):1851–63.
14. Serra V, Markman B, Scaltriti M, et al. NVP-BEZ235, a dual PI3K/mTOR inhibitor, prevents PI3K signaling and inhibits the growth of cancer cells with activating PI3K mutations. *Cancer Res* 2008;68(19):8022–30.

15. Sakaue-Sawano A, Kurokawa H, Morimura T, et al. Visualizing spatiotemporal dynamics of multicellular cell-cycle progression. *Cell* 2008;132(3):487–98.
16. Brachmann SM, Hofmann I, Schnell C, et al. Specific apoptosis induction by the dual PI3K/mTor inhibitor NVP-BEZ235 in HER2 amplified and PIK3CA mutant breast cancer cells. *Proc Natl Acad Sci USA* 2009;106(52):22299–304.
17. Fingar DC, Salama S, Tsou C, Harlow E, Blenis J. Mammalian cell size is controlled by mTOR and its downstream targets S6K1 and 4EBP1/eIF4E. *Genes Dev* 2002;16(12):1472–87.
18. Bondar VM, Sweeney-Gotsch B, Andreeff M, Mills GB, McConkey DJ. Inhibition of the phosphatidylinositol 3'-kinase-AKT pathway induces apoptosis in pancreatic carcinoma cells in vitro and in vivo. *Mol Cancer Ther* 2002;1(12):989–97.
19. Semba S, Itoh N, Ito M, Harada M, Yamakawa M. The in vitro and in vivo effects of 2-(4-morpholinyl)-8-phenyl-chromone (LY294002), a specific inhibitor of phosphatidylinositol 3'-kinase, in human colon cancer cells. *Clin Cancer Res* 2002;8(6):1957–63.
20. O'Brien C, Wallin JJ, Sampath D, et al. Predictive biomarkers of sensitivity to the phosphatidylinositol 3' kinase inhibitor GDC-0941 in breast cancer preclinical models. *Clin Cancer Res* 2010;16(14):3670–83.
21. Dan S, Okamura M, Seki M, et al. Correlating phosphatidylinositol 3-kinase inhibitor efficacy with signaling pathway status: in silico and biological evaluations. *Cancer Res* 2010;70(12):4982–94.
22. Frost P, Moatamed F, Hoang B, et al. In vivo antitumor effects of the mTOR inhibitor CCI-779 against human multiple myeloma cells in a xenograft model. *Blood* 2004;104(13):4181–7.
23. Yu K, Shi C, Toral-Barza L, et al. Beyond rapalog therapy: preclinical pharmacology and antitumor activity of WYE-125132, an ATP-competitive and specific inhibitor of mTORC1 and mTORC2. *Cancer Res* 2010;70(2):621–31.
24. Pollizzi K, Malinowska-Kolodziej I, Stumm M, Lane H, Kwiatkowski D. Equivalent benefit of mTORC1 blockade and combined PI3K-mTOR blockade in a mouse model of tuberous sclerosis. *Mol Cancer* 2009;8:38.
25. Kong D, Dan S, Yamazaki K, Yamori T. Inhibition profiles of phosphatidylinositol 3-kinase inhibitors against PI3K superfamily and human cancer cell line panel JFCR39. *Eur J Cancer* 2010;46(6):1111–21.

Bioorganic & Medicinal Chemistry 20 (2012) 1947–1951

Contents lists available at SciVerse ScienceDirect

Bioorganic & Medicinal Chemistry

journal homepage: www.elsevier.com/locate/bmc

JFCR39, a panel of 39 human cancer cell lines, and its application in the discovery and development of anticancer drugs

Dexin Kong [a], Takao Yamori [b,*]

[a] Tianjin Key Laboratory on Technologies Enabling Development of Clinical Therapeutics and Diagnostics, School of Pharmaceutical Sciences and Research Center of Basic Medical Sciences, Tianjin Medical University, Tianjin 300070, China
[b] Division of Molecular Pharmacology, Cancer Chemotherapy Center, Japanese Foundation for Cancer Research, 3-8-31 Ariake, Koto-ku, Tokyo 135-8550, Japan

ARTICLE INFO

Article history:
Available online 21 January 2012

Keywords:
JFCR39
Cancer cell line panel
COMPARE analysis
Drug discovery and development
ZSTK474

ABSTRACT

Over the past few decades, panels of human cancer cell lines have made a significant contribution to the discovery and development of anticancer drugs. The National Cancer Institute 60 (NCI60), which consists of 60 cell lines from various human cancer types, remains the most powerful human cancer cell line panel for high throughput screening of anticancer drugs. The development of JFCR39, comprising a panel of 39 human cancer cell lines coupled with a drug-activity database, was based on NCI60. Like NCI60, JFCR39 not only provides disease-oriented information but can also predict the action mechanism or molecular target of a given antitumor agent by utilizing the COMPARE algorithm. The molecular targets of ZSTK474 as well as several other antitumor agents have been identified by using JFCR39 and some of these compounds have since entered clinical trials. In this review, we will describe human cancer cell line panels particularly JFCR39 and its application in the discovery and/or development of anticancer drug candidates.

1. Introduction

Discovery and development of new anticancer drugs require a reliable predictive preclinical model to test drug efficacy. Such models mainly include human cancer cell lines propagated in culture or as xenografts in mice, and genetically engineered mouse models of human caricinogenesis.[1] The need for high throughput and low cost means that only the cultured human cancer cell line model is applicable in both drug discovery and drug development. The other models are generally used only in the drug development process.[1] Indeed, cultured human cancer cell lines have been widely used for decades as a disease-oriented screening model for new anticancer drugs. In the past ten years, development of molecular-targeted anticancer drugs has been a great success (e.g., development of imatinib). These drugs are generally designed to target oncogene-encoding-proteins specifically or far more expressed in cancer cells. Genomic heterogeneity has been frequently reported to exist across the patient population with the same pathological cancer type, and some oncogenes have been known to play a key role in tumorigenesis. In order to match the 'right' drugs to the 'right' patient, a predictive biomarker is required for molecular-targeted drugs. Cell line panels of a certain cancer type have been used to discover these predictive biomarkers.[2] As an example, PIK3CA mutation and EGFR amplification have been demonstrated to be predictive biomarkers of a PI3K inhibitor GDC-0941 by use of a large panel of breast cancer cell lines with or without PIK3CA mutation and EGFR amplification.[2] Recently, a huge panel named CMT1000 (Center for Molecular Therapeutics1000), which currently consists of 1200 human cancer cell lines, was established for the development of molecular-targeted drugs against various cancers. This panel of cell lines is expected to evaluate the sensitivity of inhibitors targeting EGFR, ERB2, MET, PDGFR, ALK and BRAF kinases.[1]

NCI60 (National Cancer Institute 60),[3] which was developed in the late 1980s and consists of 60 cell lines from various human cancer types, remains the most powerful human caner cell panel for high throughput screening of anticancer drugs. In addition to the disease-oriented screening of anticancer drugs, which was the original aim for establishment of NCI60, another function of this cancer cell line panel system is the prediction of action mechanism of antitumor agents. This latter function contributed to the development of bortezomib, an inhibitor of proteasome that was approved in 2003 by the US Food and Drug Administration (FDA). Compared with NCI60, JFCR39 (Japanese Foundation for Cancer Research 39) is a more compact system with a reduced number of cell lines. Nonetheless, JFCR39 retains the functional capability of NCI60.

* Corresponding author. Tel.: +81 3 3520 0111.
E-mail address: yamori@jfcr.or.jp (T. Yamori).

0968-0896/$ - see front matter © 2012 Elsevier Ltd. All rights reserved.
doi:10.1016/j.bmc.2012.01.017

2. JFCR39, an informatic anticancer drug discovery and development system

The development of JFCR39 in the early 1990s was based on the NCI60 system with some modification.[4,5] Like NCI60, this system consists of a human cancer cell line panel coupled with a drug-activity database. The JFCR39 panel utilizes 30 cell lines in NCI60 together with 6 cell lines of stomach cancer of which the incidence is high in Japan, and 3 breast cancer cell lines (HBC-4, HBC-5, and BSY-1) established in JFCR (Japanese Foundation for Cancer Research) (see Table 1).[4,5] Genomics on each cell line of JFCR39 has been recently reported.[6]

Like NCI60, one important function of JFCR39 is to evaluate the in vitro drug efficacy and provide disease-oriented information based on the differential growth inhibition activity of a certain antitumor agent against the 39 cancer cell lines. Inhibition of cell growth is assessed by the sulforhodamine B (SRB) assay, which determines the change in total cellular protein of the cells following 48 h of treatment with the antitumor agent.[7–9] The molar concentration of the agent needed for 50% growth inhibition (GI50) of each cell line in JFCR39 is then obtained.[9,10] A graphical representation (or 'fingerprint') for the differential growth inhibition against the cells in the JFCR39 panel is finally plotted based on a calculation that uses a set of GI50 values.[11]

Another function of the JFCR39 is to predict the action mechanism or molecular target of an antitumor agent. The action mechanism of a drug candidate can be predicted by comparing its fingerprint with those of reference compounds (including anticancer drugs and chemical tools with known mechanisms) in our drug-activity database using the COMPARE algorithm, because the fingerprint represents the whole inhibition profile of the growth-related targets in the cells.[5,9] The COMPARE analysis is carried out by calculating the Pearson correlation coefficient (r value) between the GI50 mean graphs of two compounds X and Y using the following formula: $r = (\sum(x_i - x_m)\ (y_i - y_m))/(\sum(x_i - x_m)^2 \sum(y_i - y_m)^2)^{1/2}$, where x_i and y_i are Log GI50 of the two compounds, respectively, for each cell line, and x_m and y_m are the mean values of x_i and y_i, respectively ($n = 39$).[9,11] The r value is then used to determine the degree of similarity, that is, the higher the r value is, the greater the similarity of X with Y. Generally, an r value of more than 0.6 between two agents suggests they might have a similar action mechanism, whereas a value of >0.8 suggests they have the same mechanism of action. Interestingly, we recently found that the difference of r value between 0.6 and 0.8 might reflect the different target specificity between two phosphatidylinositol 3-kinase (PI3K) inhibitors.[12]

Table 1
Cell lines in JFCR39 panel

Cancer	Number of cell lines	Cell line
Lung	7	NCI-H23, NCI-H226, NCI-H522, NCI-H460 A549, DMS273, DMS114
Stomach	6	St-4, MKN-1, MKN-7, MKN-28, MKN-45, MKN-74
Ovarian	5	OVCAR-3, OVCAR-4, OVCAR-5, OVCAR-8, SK-OV-3
Renal	2	RXF-631L, ACHN
Melanoma	1	LOX-IMVI
Colon	5	HCC-2998, KM-12, HT-29 HCT-15, HCT-116
Breast	5	*HBC-4, BSY-1, HBC-5* MCF-7, MDA-MB-231
Brain	6	U251, SF-268, SF-295, SF-539, SNB-75, SNB-78
Prostate	2	DU-145, PC-3

The cell lines underlined are stomach cancer cell lines with high incidence in Japantyped and those in italics are established in JFCR.

3. Application of JFCR39 in the discovery and development of anticancer drugs

3.1. FJ5002

We have been searching for new anticancer drug candidates in our database by using JFCR39 COMPARE analysis-guided assay. As an example, FJ5002 (CAS number 147366-40-3, Fig. 1) was discovered as a potent telomerase inhibitor in 1999.[13] To search for a potent telomerase inhibitor in our drug-activity database, we used berberine, a compound which weakly inhibits telomerase with an IC50 of 37 μM, as a seed compound. The COMPARE analysis with JFCR39 generates a list of top 20 compounds with r values of more than 0.6. Then we determined their telomerase inhibitory activity and found MKT077 was a more potent telomerase inhibitor (IC_{50}: 5 μM) than berberine. We then performed another round of COMPARE analysis by using MKT077 as a seed compound. Subsequently, another list of top 20 compounds exhibiting higher r values than 0.6 was produced. An assay of their telomerase inhibitory activity led to the discovery of FJ5022 as a more potent telomerase inhibitor than MKT077. FJ5002 inhibits telomerase with an IC_{50} of 2 μM, causes population-doubling dependent changes characterized by progressive telomere erosion, increased chromosome abnormalities and senescence/crisis-like features in long-term cultivated U937 cells.[13]

3.2. Pladienolide B

The JFCR39 system can be used to determine the action mechanism or molecular target of an antitumor agent. Of course, prediction of a molecular target depends on whether there is a reference compound with the same molecular target in the database. If not, we can predict that the compound has a novel molecular target, which is different from that of current drugs or chemical tools. Pladienolide B is one such example.[14]

Pladienolide B (see Fig. 1) is a 12-membered macrolide isolated from *Streptomyces platensis* Mer-11107 by scientists of Eisai. This compound exhibits potent growth inhibitory activity against various cell lines including those resistant to chemotherapeutic drugs like camptothecin, and induces cell cycle arrest at both G1 and G2/M. Favorable in vivo antitumor activity of pladenolide B iv was also shown on xenograft models such as WiDr and BSY-1. To investigate the molecular target of pladienolide B, COMPARE analysis was carried out by use of our JFCR39 system. However, there were no compounds in our reference list with an r value greater than 0.6, suggesting pladienolide B has a novel molecular target or mechanism.[14] Based on this interesting finding, continuous efforts were made to investigate the molecular target of pladienolide B. Finally, by use of ^{3}H-labeled, fluorescence-tagged and photoaffinity/biotin (PB)-tagged chemical probes, splicing factor SF3b was demonstrated to be the target protein of this agent.[15] Currently, a derivative of pladienolide B, E7107, is under evaluation in clinical trials for cancer treatment.

3.3. MS-247

The first example of the use of JFCR39 to determine a molecular target was for the synthetic compound MS-247 (see Fig. 1).[9] COMPARE analysis predicted that this compound might target topoisomerase because an r value of 0.683 was shown for correlation with CPT-11, a well known topoisomerase inhibitor. Such a prediction was then demonstrated by the result that MS-247 inhibited the topoisomerase-induced conversion of supercoiled DNA to nicked

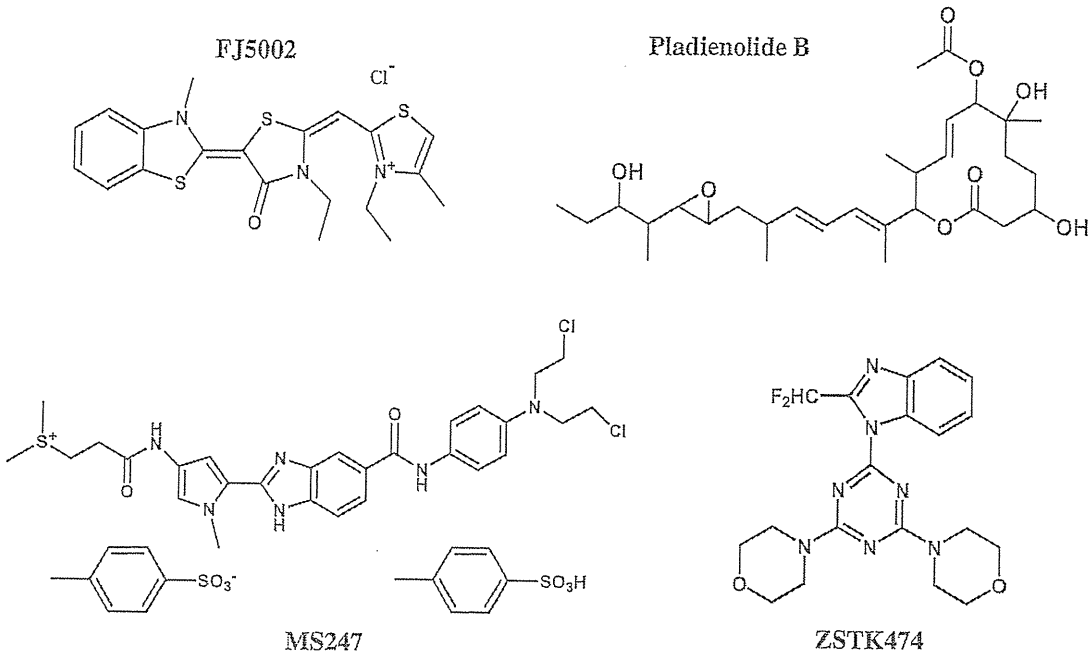

Figure 1. Chemical structures of the representative compounds identified by JFCR39.

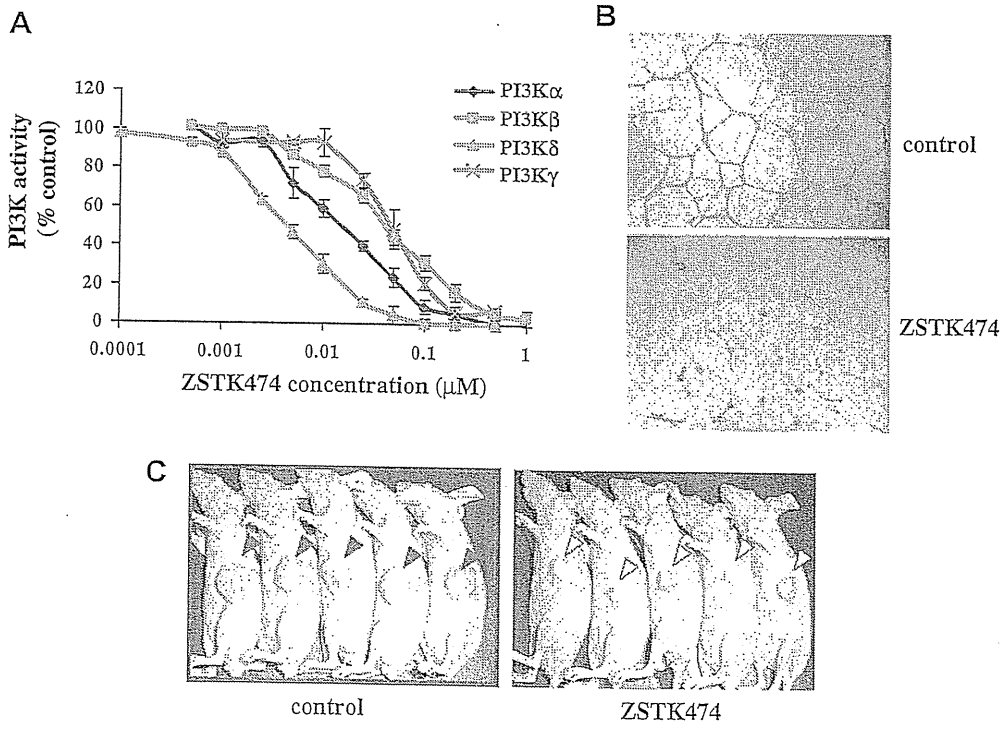

Figure 2. PI3K inhibition and antitumor activities of ZSTK474. (A) Inhibitory activity of ZSTK474 against class I PI3K isoforms. (B) In vitro antiangiogenic activity of ZSTK474. ZSTK474 (1 μM) inhibits tube formation by HUVEC (human umbilical vein endothelial cell). Quantitative data can be seen in previous report.[23] (C) In vivo antitumor efficacy of ZSTK474. Oral administration of ZSTK474 at 400 mg/kg to WiDr xenograft daily from day 0 to 26, except for days 6, 13 and 20, leads to obvious tumor growth inhibition. The pictures were taken on day 28.

DNA.[9] In addition, MS-247 exhibited an average IC_{50} of 0.71 μM for 39 cancer cell lines as well as inducing cell cycle arrest at G2/M phase and apoptosis at a concentration of 0.1 μM.[9] Based on these results, MS-247 was examined for the antitumor activity and found to exhibit potent in vivo antitumor efficacy on 17 xenografts derived from JFCR39.[9]

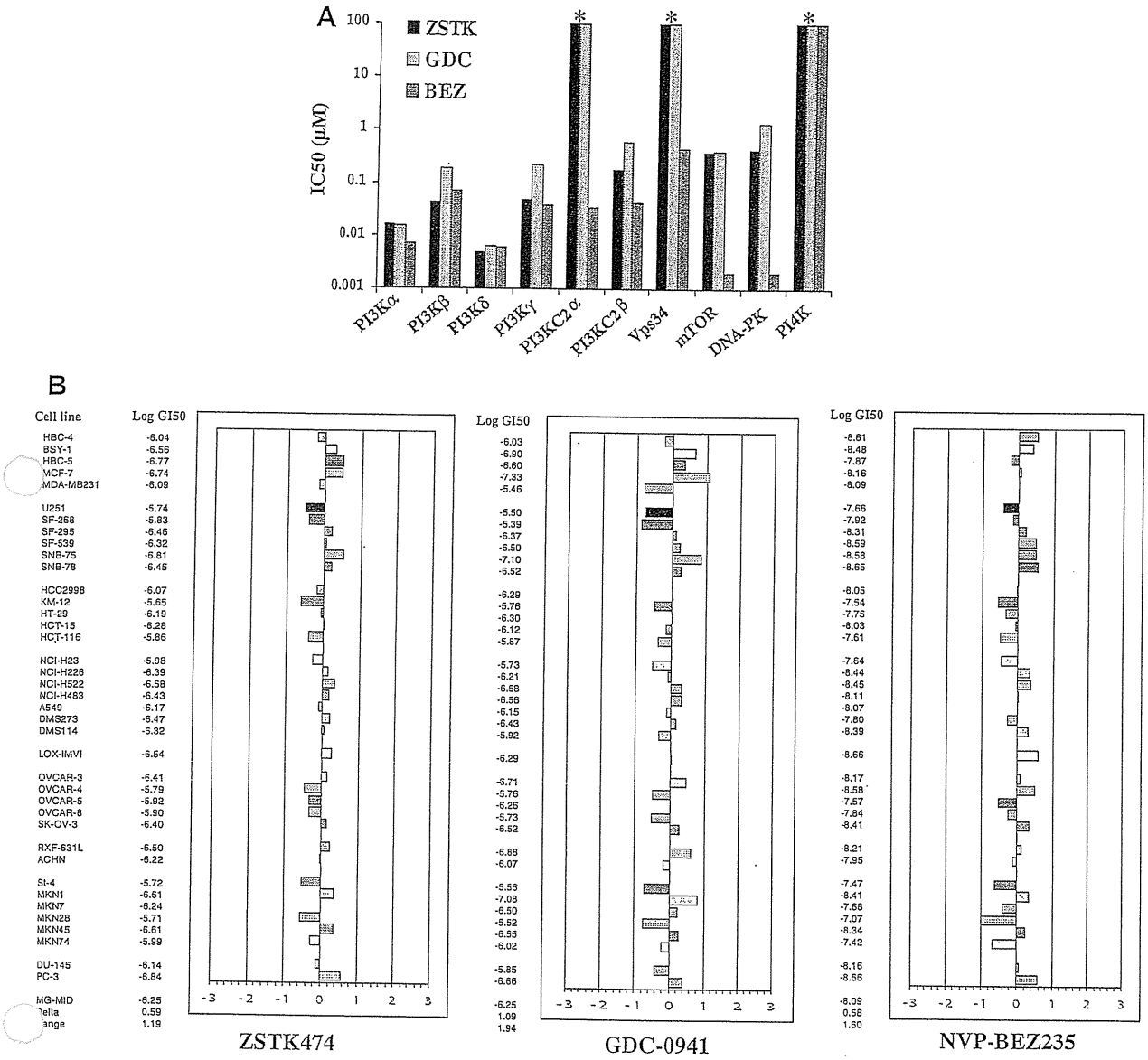

Figure 3. Similarity between JFCR39 fingerprints of PI3K inhibitors can be used to predict related target specificities. (A) Inhibition profiles of PI3K inhibitors ZSTK474, GDC-0941 and NVP-BEZ235 against PI3K superfamily members. The IC50 values of the respective PI3K inhibitor for each kinase were used to plot the inhibition profile, *: >100. ZSTK474 has a similar class I PI3K inhibitory specificity with GDC-0941, but different from NVP-BEZ235. (B) JFCR39 fingerprints of PI3K inhibitors ZSTK474, GDC-0941 and NVP-BEZ235. The ZSTK474 fingerprint exhibits a greater similarity to the fingerprint of GDC-0941, than that of NVP-BEZ235. Fingerprint indicates the differential growth inhibition pattern of ZSTK474 for the cell lines in the JFCR39 panel. The X-axis shows the difference in logarithmic scale between the mean of LogGI50 values for all 39 cell lines (MG-MID, expressed as 0 in the fingerprint) and the LogGI50 for each cell line in the JFCR39 panel. Columns to the right of 0 indicate the sensitivity of the cell lines to a given compound and columns to the left indicate their resistance. MG-MID = mean of LogGI50 values for all 39 cell lines; Delta = difference between the MG-MID and the LogGI50 value for the most sensitive cell line; Range = difference between the LogGI50 values for the most resistant cell line and the most sensitive cell line.

3.4. ZSTK474

To date, the most successful application of JFCR39 has been the identification of ZSTK474 (CAS number 475110-96-4, Fig. 1) as a PI3K inhibitor. ZSTK474 is an s-triazine derivative that was originally synthesized by Zenyaku Kogyo as an anticancer drug candidate.[16] This compound showed the most promising antitumor efficacy among over 1500 synthesized analogues. However, the molecular target was unknown. In 2003, growth inhibitory activity of ZSTK474 was examined against the JFCR39 panel and its corresponding fingerprint was developed. COMPARE analysis was then carried out by comparing the fingerprint of ZSTK474 with those of reference compounds in the JFCR39 drug-activity database. Interestingly, a high r value of 0.766 was found between the fingerprint of ZSTK474 and that of LY294002, a well known class I PI3K inhibitor.[17] We then predicted that ZSTK474 might also target class I PI3K. Class I PI3K is a family of four lipid kinase isoforms that phosphorylate phosphatidylinositol 4,5-bisphosphate (PIP2) to generate phosphatidylinositol 3,4,5-trisphosphate (PIP3), which plays an important role in various processes including cell growth.[18–20] To demonstrate that ZSTK474 really targets PI3K, we investigated the activity of the recombinant class I PI3K isoforms in the absence or presence of ZSTK474 by use of a homogeneous time-resolved fluorescence (HTRF) assay. Our results showed that ZSTK474